Towards scalable organ-level 3D plant segmentation: Bridging the data-algorithm-computing gap

Ruiming Du^a, Guangxun Zhai^b, Tian Qiu^c and Yu Jiang^{b,*}

ARTICLE INFO

Keywords: Point cloud segmentation Plant Phenotyping Quantitative review Benchmark Sim-to-real

ABSTRACT

The precise characterization of plant morphology provides valuable insights into plant-environment interactions and genetic evolution. A key technology for extracting this information is 3D segmentation, which delineates individual plant organs from complex point clouds. Despite significant progress in general 3D computer vision domains, the adoption of 3D segmentation for plant phenotyping remains limited by three major challenges: i) the scarcity of large-scale annotated datasets, ii) technical difficulties in adapting advanced deep neural networks to plant point clouds, and iii) the lack of standardized benchmarks and evaluation protocols tailored to plant science. This review systematically addresses these barriers by: i) providing an overview of existing 3D plant datasets in the context of general 3D segmentation domains, ii) systematically summarizing deep learning-based methods for point cloud semantic and instance segmentation, iii) introducing Plant Segmentation Studio (PSS), an open-source framework for reproducible benchmarking, and iv) conducting extensive quantitative experiments to evaluate representative networks and sim-to-real learning strategies. Our findings highlight the efficacy of sparse convolutional backbones and transformer-based instance segmentation, while also emphasizing the complementary role of modeling-based and augmentation-based synthetic data generation for sim-to-real learning in reducing annotation demands. In general, this study bridges the gap between algorithmic advances and practical deployment, providing immediate tools for researchers and a roadmap for developing data-efficient and generalizable deep learning solutions in 3D plant phenotyping. Data and code are available at: https://github.com/perrydoremi/PlantSegStudio.

1. Introduction

Plant morphology addresses the organization of plant organs and provides the taxonomic foundation for understanding plant relationships, environmental adaptations, and genetic evolution (Simpson, 2019; Yang et al., 2020). Accurate characterization of morphological traits is essential for breeding programs and plant science research, serving as a cornerstone for advancing agricultural productivity and sustainability (Wyatt, 2016). Recent advances in imaging technologies and computer vision have enabled sensor-based measurements of morphological traits, generating objective and quantifiable data. These measurements are valuable not only for plant morphology but also for plant genetics, including quantitative trait loci (QTL) analysis, thereby facilitating crop breeding through genetics and genomics approaches. In particular, recent studies have been conducted to extend imaging-based measurements of plant morphological traits from conventional field or whole-plant scales (e.g., plant or plot height) to organ-level resolution (e.g., internode distance or flower and fruit distribution). Access to organlevel traits creates new opportunities to deepen understanding in plant biology and broader life sciences, while also supporting efforts to improve crop adaptability and therefore agriculture resilience to diverse environments (Li et al., 2022b; Jin et al., 2021).

*Corresponding author Email address: yujiang@cornell.edu Image segmentation is a key step to extract plant morphological traits at the organ level. Early attempts at imaging-based plant morphology phenotyping have heavily relied on 2D imaging techniques due to the relative ease of image acquisition through RGB cameras and the widespread availability of image segmentation algorithms. These algorithms include both classical computer vision techniques such as thresholding (Easlon and Bloom, 2014) and edge detection-based segmentation (Wang et al., 2018d) and learning-based methods such as convolution neural networks (CNNs) that leverage large annotated image datasets and computing power (Jiang and Li, 2020). However, 2D imaging-based solutions are highly constrained by the view dependency and the insufficiency of resolving occlusion. Therefore, many recent attempts have focused on 3D imaging techniques.

Among possible representation formats, 3D point clouds have gained substantial popularity in 3D plant phenotyping because they explicitly capture raw 3D coordinates of a scene that can be directly obtained from sensors such as LiDARs while preserving high spatial details. Further, acquiring full-view 3D point clouds dramatically reduces, if not fully avoids, measurement errors caused by view-dependency and occlusion. Similar to 2D imaging-based solutions, 3D point cloud segmentation plays a vital role in the extraction of plant morphological traits. In general, 3D point cloud segmentation can also be categorized as 3D semantic and instance segmentation. 3D semantic segmentation aims to assign a semantic class label to every point in a 3D point cloud, thereby providing a comprehensive

^aDepartment of Biological and Environmental Engineering, Cornell University, Ithaca, 14850, NY, USA

^bHorticulture Section, School of Integrative Plant Science, Cornell AgriTech, Cornell University, Geneva, 14456, NY, USA

^cSchool of Electrical and Computer Engineering, Cornell University, Ithaca, 14850, NY, USA

mapping of plant organ semantics. The segmentation results enable the analysis of basic organ-level relationships such as hierarchical canopy architecture, leaf-stem ratios, and organ distribution patterns. These traits are essential for studying light interception for photosynthesis, modeling plant resource allocation, and understanding overall organ growth (Zhu et al., 2020; Conn et al., 2017a; Li et al., 2025a; Jin et al., 2019). 3D instance segmentation distinguishes between different individual instances of the same class (e.g., identifying and separating each leaf or fruit). The instance segmentation result allows the analysis of intricate spatial arrangements and variation among specific organs. For example, 3D instance segmentation has been used for organ counting, analysis of organ size, shape, and orientation, and organ development and growth (Zhang et al., 2024; Li et al., 2024a; Mirande et al., 2022).

In early stages, efforts on 3D point cloud segmentation concentrated on semantic segmentation (Xie et al., 2020). Traditional methods primarily combine hand-crafted features such as point feature histograms (PFH), curvature, and point and surface normal (Rusu et al., 2008; Rabbani et al., 2006) with classical classifiers such as support vector machines (SVM), random forests (RFs), and Bayesian discriminators (Weinmann et al., 2015; Wang et al., 2015; Niemeyer et al., 2012) to classify the semantic meaning of each point (Maturana and Scherer, 2015; Xie et al., 2020). The success of this strategy highly relies on prior knowledge of plant geometry to design local and global features that sufficiently represent the statistical properties of plant point clouds and on exhaustive search of optimal classifiers that adequately use these features (Wang et al., 2015). In addition to these general 3D point cloud features, plant phenomics researchers actively tailored features for plant morphology, including 3D plant skeletons (Bao et al., 2019; Ma et al., 2023; Gaillard et al., 2020), leaf area index (LAI) (Itakura and Hosoi, 2018), and canopy structures (Bienert et al., 2021). Although these methods provided improved results in specific cases, they are resource-demanding for development and cannot be well generalized among plant species or applications. At the same time, 3D point cloud instance segmentation did not receive much attention. A related task is 3D detection in which the proposals (i.e., 3D bounding box) rather than point-wise masks are used for differentiating instances within the same semantic category (Chen et al., 2015; Ren and Sudderth, 2016). Later on, 3D detection inspired the early research on proposal-based 3D point cloud instance segmentation (Section 3.2.1).

Recently, deep learning (DL)-based methods have overtaken 3D point cloud semantic segmentation in various domains and have begun focusing on instance segmentation, owing to their powerful ability to learn geometric features directly from data and their superior segmentation performance (Qi et al., 2017a; Wang et al., 2018c). DL-based methods have significantly improved segmentation accuracy and shifted the research focus from feature engineering to deep neural network design across a wide range of computer vision tasks and applications, including autonomous driving,

object recognition, photogrammetry, and remote sensing. This shift has led to substantial progress in segmentation-based reasoning of 3D scenes (Sun et al., 2020a; Dai et al., 2017; Hu et al., 2021). Similar to the success of deep learning in other computer vision tasks and research fields, this improvement has been driven by advancements across the data-algorithm-computing triangle: i) the availability of large-scale annotated datasets that capture statistical patterns, ii) modern deep neural networks capable of learning features from big data, and iii) computing infrastructure (e.g., hardware, streamlined workflows, and evaluation protocols) that supports model training, evaluation, and comparison for continuous improvement.

Organ-level plant morphology phenotyping has advanced through improvements in 3D segmentation as well as broader progress across the data-algorithm-computing triangle (Li et al., 2022b,a; Jin et al., 2020; Du et al., 2023). Many recent studies in 3D plant phenotyping have employed either custom 3D imaging systems, such as automated multiview stereo systems, or advanced sensors, including LiDAR and laser scanners, to capture high-resolution plant point clouds for extracting morphological traits at the organ level. In parallel, these studies have developed analysis pipelines that leverage DL-based segmentation through supervised or semi-supervised learning schemes, demonstrating satisfactory performance. Nevertheless, the pace of organ-level 3D plant phenotyping has not been sufficient to fully realize its potential, particularly regarding processing scalability and model generalizability. These limitations highlight the need for a systematic review of current challenges and future directions in 3D plant phenotyping, framed through the perspective of the data-algorithm-computing triangle, with particular attention to the unique demands of plant sciences and agriculture.

The overarching goal of this review is to provide a systematic synthesis of recent advances in 3D point cloud segmentation for organ level plant phenotyping through the lens of the data–algorithm–computing triangle. Specifically, the review includes four major components:

- i) An in-depth overview of data collection approaches and publicly available datasets for 3D plant phenotyping at the organ level.
- ii) A comprehensive analysis of DL-based 3D point cloud segmentation methods.
- iii) Introduction of Plant Segmentation Studio (PSS), an open source framework designed to streamline benchmark analysis for 3D plant phenotyping.
- iv) Extensive quantitative experiments on benchmark datasets and representative methods to generate insights for future research.

We anticipate that this review will not only serve as a key reference for researchers across disciplines interested in DL-based point cloud segmentation for plants but also provide quantitative evidence to inform future research toward scalable 3D segmentation and analysis of organ-level plant

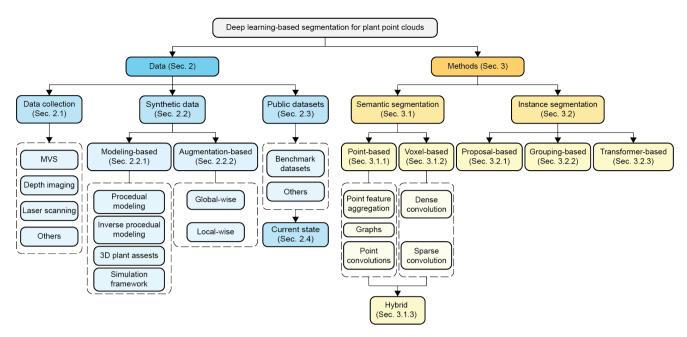


Figure 1: Review outline of deep learning-based segmentation for plant point clouds.

phenotyping, thereby advancing the understanding of fundamental life science mechanisms and supporting agricultural sustainability and resilience.

The rest of this manuscript was organized as follows: Section 2 reviews the 3D plant datasets for segmentation-based phenotyping. Section 3 reviews the key deep neural networks for point cloud semantic and instance segmentation. The outline for our review (Section 2 and Section 3) is illustrated in Fig. 1. Section 4 introduces the development of PSS. Section 5 provides the methods, experiments, and results of selected benchmark datasets, semantic and instance networks, and synthetic training data generation for sim-to-real learning. Section 6 discusses key findings and insights of network design and training strategies for different 3D plant segmentation requirements. Section 7 summarizes and provides perspectives for future directions in 3D segmentation-based plant phenotyping.

2. 3D plant data collection and synthetic data generation for segmentation

In this section, we reviewed data generation (both data collection and synthetic generation) and publicly available datasets for 3D plant morphology phenotyping, especially at the organ level. While there are many 3D point cloud datasets for plants, the majority of these datasets is for forestry research and forest inventory and collected using terrestrial laser scanning (TLS) (Hui et al., 2021; Shen et al., 2022; Wang, 2020; Liang et al., 2016) or aerial laser scanning (ALS) (Brede et al., 2022; Xiang et al., 2024). Analyzing these datasets primarily extracts traits at the **plant-level**, requiring the segmentation of individual trees or the segregation between foliage and woody components. The extracted traits are subsequently used for tree

species analysis (Henrich et al., 2024; Terryn et al., 2020; Xi et al., 2020), biomass estimation (Van den Broeck et al., 2023; Brede et al., 2022; Demol et al., 2022), and foliage property characterization such as foliage density and leaf angle distribution (LAD) (Mkaouar et al., 2021; Zheng et al., 2013; Fang et al., 2019; Wang and Fang, 2020). Within the context of plant phenotyping for agricultural crops, the research interests have been shifted from extracting traits at the plant-level to the **organ-level** where plant organs (e.g., stem, branch, leaf, flower, and fruit) need to be segmented individually within a single plant. As we aimed to review plant phenotyping for agricultural crops at the organ-level, we only summarized datasets that consist of 3D point clouds with organ-level annotation for agricultural crops in this section.

2.1. Real world data acquisition

Organ-level plant segmentation forms the basis for characterizing detailed plant morphological traits and requires high-quality point clouds. Collecting such datasets mainly uses photogrammetry-based solutions such as multi-view stereo and specialized sensors such as depth cameras and laser scanners.

Photogrammetry-based 3D reconstruction is widely used for plant phenotyping because of its affordability and utility, especially multi-view stereo (MVS). MVS reconstructs the 3D structure of a scene using a set of images captured from multiple overlapping viewpoints. Given the camera pose for each image either obtained through hardware configuration or estimated computationally such as using structure from motion (SfM), MVS can compute depth information and generate a detailed 3D reconstruction of the scene from these multiple perspectives.

SfM-MVS pipeline is highly flexible to deal with various data collection scenarios from controlled environment agriculture (CEA) to in-the-wild environment with consumergrade RGB cameras or even smartphones (Mertoğlu et al., 2023; Zhu et al., 2024; Sun et al., 2020b; Xiao et al., 2020; Wang et al., 2022b; Gao et al., 2021). However, the geometric accuracy and resolution of the final 3D data are sensitive to the images quality, the number of viewpoints, and collection environment. Poor texture, insufficient views, or movement of the plant organs will more likely lead to incomplete or inaccurate point clouds. Compared to SfM-MVS, a more robust and repeatable implementation, specifically for CEA environment, is MVS-based high-throughput platforms (HTP) with known camera poses and controlled rotation or movement of plants. Bypassing the SfM and proving precise camera intrinsic and extrinsic parameters, this implementation significantly increases the speed and quality of reconstructed 3D plant data (Wu et al., 2020; Sun et al., 2023b; Li et al., 2022c; Wu et al., 2022).

Depth cameras (e.g., Time-of-Flight (ToF), structured light, and stereo vision-based) offer a cost-effective and rapid approach for point cloud collection, especially the development of consumer-grade products (Microsoft Kinect, Intel RealSense, and Orbbec series), which have revolutionized access to 3D imaging by significantly reducing the costs (Song et al., 2023). However, they generally suffer from a shorter optimal sensing range and are susceptible to ambient light conditions, and are often integrated into phenotyping platforms (Ma et al., 2019; Gong et al., 2021) or robotics (Xie et al., 2024; Xu and Li, 2022) in laboratories or greenhouses. Such a trade-off makes the plant point cloud stand out in two aspects with different properties: On one hand, the data usually represents potted plants with simple structures for CEA with low resolution and quality compared to laser scanning imaging (Chéné et al., 2012; Li et al., 2022b; Song et al., 2025). On the other hand, the excellent operational simplicity of depth cameras makes the data capable of describing finer temporal-spatial resolution to enable an easier approach for plant growth monitoring (Khanna et al., 2019; Hamamoto et al., 2020; Bernotas et al., 2019). In addition, the well-established depth calibration methods make the data more feasible to fuse with other modalities (e.g., multispectrum, thermal, rgb) to generate multi-modality 3D point clouds (Xie et al., 2023; Qiu et al., 2021; Wang et al., 2023) for studying plant spatial physiology.

Laser scanning encompasses a range of active sensing technologies that obtain 3D information by emitting laser light and analyzing the properties of the reflected signal to determine precise distances to objects. In general, laser scanning takes the leading role in providing high-quality organ-level datasets due to its outstanding capability to capture finer morphological features (e.g., leaf curvature, stem thickness, rice spikes) to generate high-resolution and accurate plant point clouds compared to other modalities. (Han et al., 2021; Song et al., 2025; Guo et al., 2021; Jin et al., 2021). However, given specific laser scanning technologies, the capability for detailing plant organs and

the collection scale varies. Currently, there are three main technologies predominant for 3D plant imaging (Stausberg et al., 2024): Terrestrial laser scanning (TLS) involves stationary systems that scan statistic scenes from fixed positions (Oiu et al., 2024b; Jin et al., 2019; Yun et al., 2025); Highly commercialized handheld laser scanners (HLS), which offer excellent portability and flexibility for small scale 3D imaging (Ma et al., 2023; Du et al., 2023); and mobile laser scanning (MLS) systems, which are usually mounted on various platforms and synergized with georeferencing techniques for large plots or in-the-field 3D imaging (Sun et al., 2017; Tiozzo Fasiolo et al., 2023; Xu and Li, 2022; Sun et al., 2018). Notable trade-offs are associated with these technologies. Data collection with TLS can be time-consuming due to the need for multiple scan positions, followed by coregistration to mitigate occlusion and cover the entire scene (Qiu et al., 2024a). While HLS systems reduce occlusion issues compared to static TLS by allowing dynamic scanning around the plant, they require dedicated manual operation for scanning view adjustment, often achieving less throughput compared to TLS and MLS approaches, and are usually used for a single plant in CEA environments (Yang et al., 2024). MLS usually achieves less precision compared to TLS or HLS approaches, given the extra registration errors from georeferencing and laser sensors that sacrifice accuracy for throughput in the field (Esser et al., 2023; Qiu et al., 2019).

Beyond the commonly used depth cameras, MVS, and laser scanning for 3D plant data collection, other specialized techniques, such as X-ray scanning, offer unique capabilities for studying occlusion-free geometry of plant shoot (Dutağacı et al., 2020; Turgut et al., 2022), root system (Atkinson et al., 2019; Freschet et al., 2021; Tracy et al., 2020) or achieving ultra-high spatial resolution for tiny organs (Staedler et al., 2013; Wang et al., 2017; Du et al., 2016; Lowry et al., 2024).

In summary, the optimal data collection for specific phenotyping goals hinges on careful assessments of the target plant species, organ characteristics, accuracy, and resolution requirements. No single approach or data format is universally superior, rather, it's a fitness-for-purpose weighing. Besides, different scenarios will bring different challenges for segmentation. For example, sparse point clouds representing plants with regular or simple structures are typically more amenable to segmentation, with even lightweight network architectures capable of achieving near-optimal performance. In contrast, dense point clouds with complex geometries demand models with stronger local geometric reasoning or computationally efficient algorithms to process highdensity data. Likewise, organs with distinct morphologies, such as broad, round leaves versus thin, elongated branches, may require different instance segmentation strategies to achieve robust performance (Discussed in Section 5.3).

Regardless of the sensing modality or networks employed, the availability of annotated training data remains a critical factor for the success of DL-based segmentation.

However, the costly nature of manual annotation continues to limit the broader adoption of advanced DL techniques in plant phenotyping. To address this limitation, the community is pursuing a dual-track strategy: on one hand, enhancing high-throughput, cost-effective imaging systems and expanding high-quality real-world datasets. On the other hand, exploring synthetic data generation to support sim-to-real (sim2real) transfer learning.

2.2. Synthetic data generation

Synthetic data generation can produce large volumes of diverse 3D plant data with perfect, automatically generated ground truth labels, effectively alleviating the annotation burden. 3D plant generation is a broad field including research on functional-structural plant models (FSPMs) for simulating genotype-by-environment (G×E) interactions (Vos et al., 2010). This review section specifically focuses on synthesis for sim2real plant phenotyping: A strategy that involves training models on synthetic data to solve real-world downstream tasks. In this context, two widely used pipelines are discussed: **procedural modeling-based** (**PM-based**), which simulates plant morphology and sensor interactions from models, and **augmentation-based**, which leverage existing real-world data to create synthetic variants.

2.2.1. *PM-based*

Early endeavors in 3D synthetic plant generation extensively rely on procedural modeling (PM), with the Lindenmayer system (L-system) and its extension for plant topology simulation being milestones and foundation (Lindenmayer, 1968; Prusinkiewicz, 1986; Smith, 1984). L-systems employ a set of grammatical rules that can effectively simulate complex branching structures and capture the developmental topology nature inherent in many plants (Prusinkiewicz and Lindenmayer, 1990). With the latter efforts expanding the Lsystems' capability to model the interactions between plant parts and their response to the environment (Prusinkiewicz et al., 1993; Měch and Prusinkiewicz, 1996), L-systems are excellent and have been widely used to generate synthetic plants with high biological plausibility (Lee et al., 2023; Chaudhury et al., 2020). However, driving the procedural models or rules in PM is very demanding and tedious, requiring domain expertise for various manual parameterization (Cournède, P.-H. et al., 2011; Wang et al., 2018a).

To overcome the parameter tuning challenges stemming from most PM pipelines, inverse procedural modeling (IPM) has become the focus (Stava et al., 2014). Unlike PM, IPM automates the optimization of procedural models or rules from real-world observations and has fertilized a lot of research on generating 3D synthetic plants for sim2real in plant phenotyping (Turgut et al., 2022; Qiu et al., 2024b, 2025; Qian et al., 2023; Zhai et al., 2024; Song et al., 2019; Zarei et al., 2024). Although IPM has demonstrated great capability in generating annotated data, it still requires efforts to choose and calibrate the procedural models. Another alternative is sampling point clouds from existing 3D plant assets. However, most of these plant models are artistically

designed for animation purposes, with the priority in virtual realism rather than biological plausibility. Besides, the organ-level annotations are usually not guaranteed, and a post process for labeling is required (Wang et al., 2022a; Li et al., 2024c).

For most PM-based approaches, the key limitation hindering their full potential in sim2real application is the discrepancy between the properties of synthetic training data and real-world test data, i.e., the reality gap. It has been demonstrated that introducing the knowledge from source domains can help improve the sim2real performance (Wang and Deng. 2018). Under this inspiration, recent advances combine plant modeling with simulation frameworks (e.g., Gazebo, Helios, Helios++) to simulate the plant population and the physics of sensor interactions, e.g., how LiDAR beams propagate, reflect with the plant models in the field (Winiwarter et al., 2022). This combined pipeline can generate synthetic plant point clouds with imperfections such as occlusion and sensing effects that are more directly comparable and transferable to real sensor data, aiming to bridge the reality gap (Oiu et al., 2025; Bryson et al., 2023; Tang et al., 2024).

2.2.2. Augmentation-based

In contrast to PM-based pipelines, augmentation-based pipelines modify existing real-world point clouds to generate synthetic variants. The primary objective is to expand the size and diversity of limited training datasets, thereby enhancing the robustness and generalization capabilities of deep learning models. Specifically, augmentationbased pipelines can be divided into global-wise and localwise according to the transformation scope (Hahner et al., 2022). Global-wise transformations applied to entire point clouds include rotation, which alters plant orientation; scaling, which changes overall plant size; translation, which shifts the plant's spatial position; jittering, which adds small random noise to points; and more recently, different downsampling strategies tailored for plant point clouds (Li et al., 2024b, 2023). Most of these techniques are cost-effective and do not fundamentally alter the plant's intrinsic structure. which is often used on-the-fly while training the deep neural networks (Schunck et al., 2021; Ao et al., 2022). Local-wise methods are becoming an emerging topic for 3D plant phenotyping. They apply local transformations targeting specific plant organs. Such techniques are able to simulate a more natural variability (e.g., different leaf angles, positions, or sizes) or even simplified growth processes through hierarchically transforming certain organs, demonstrating great efficiency in increasing data diversity without the substantial efforts of procedural modeling or sensor simulation (Xin et al., 2023; Yang et al., 2024).

However, a persistent challenge within sim2real learning is how to bridge the reality gap. PM-based methods offer high control and the potential to generate biologically plausible data, but can be complex to develop, whereas augmentation-based techniques are often simpler to implement and have higher potential to create unrealistic data, but

may be constrained by the diversity of the initial real dataset. This necessitates careful validation of better training strategies with domain adaptation or randomization techniques for sim2real learning (Wang and Deng, 2018; Tobin et al., 2017; James et al., 2018; You et al., 2022).

2.3. Publicly available organ-level 3D plant datasets

An overview of 3D plant datasets that are publicly accessible is summarized in Table 1. Based on data creation method, these datasets are categorized as real-world datasets collected using various 3D imaging techniques or synthetic datasets generated through 3D data synthesis and modeling. Among these datasets, five real world datasets contain annotation for both semantic and instance segmentation at the organ level and are denoted with the asterisk symbol in Table 1. A brief description for each of the five datasets is provided below to help gain a basic understanding of their data acquisition method (and therefore data quality), data size, and intended purpose in 3D plant phenotyping.

- COS: Cornell orchard single-tree (COS) includes 98 apple tree point clouds from two orchards. Specifically, 48 Gala-W apple trees were grown at Cornell campus orchard (latitude:42.445 N, longitude: 76.462 W) in Ithaca, NY, USA, and 50 apple trees (29 of NY1-SnapDragon, 21 of NY2-RubyFrost) were grown in Cornell Agritech research orchard (latitude: 42.880 N, longitude: 77.006 W) in Geneva, NY, USA. The data collection in both orchards were conducted during the offseason with the maximum visibility of tree trunks and branches through laser sacnning (FARO Focus S350, FARO Technologies Inc., Lake Mary, FL, USA).
- HR3D: HR3D contains 546 point clouds of three crops (312 tomato, 129 sorghum, and 105 tobacco) through laser scanning (Edge Scan Arm HD, Faro Inc.), covering 20–30 days of development under 3-5 growth conditions (ambient light, shade, high heat, high light, and drought).
- SYAU-Maize: SYAU-Maize contains 428 maize point clouds of 5 varieties (Xian Yu 335, LD145, LD502, LD586 and LD 1281). During data collection, maizes were transplanted to pots and point clouds were obtained through laser scanning (FreeScan X3, Tianyuan Inc., Beijing, CN) in an indoor environment.
- Pheno4D: Pheno4D contains 128 point clouds, in which 77 point clouds of 7 tomato plants over a 20-day growth period, and 49 point clouds of 7 maize plants over a 12-day growth period. Two crops were raised in pots in a greenhouse and were measured daily through laser scanning (Perceptron Inc., Plymouth, MI, USA).
- SoybeanMVS: SoybeanMVS contains 102 soybean plant point clouds of five varieties (DN251, DN252,

DN253, HN48, and HN51) covering the whole soybean growth from the first trifoliolate stage to the full maturity stage. During data collection, 2D images from multiple viewing angles were acquired using a digital camera (Canon EOS 600D SLR, Canon (China) Co. Ltd., Beijing, CN) and subsequently used to reconstruct 3D soybean models through multi-view stereo. A total of 102 point clouds were sampled from the resultant models.

While recent efforts have produced more 3D plant datasets, their scale remains considerably smaller than that of widely used benchmark datasets in general 3D computer vision (Figure 2; compare Table 1 with Table 2). On average, only two to three new plant datasets have been released per year, although this number may increase with the continued development and deployment of high throughput phenotyping systems. This trend is promising for advancing algorithmic research in 3D plant analysis, particularly segmentation, which can accelerate plant phenomics and support applications such as crop breeding. Nevertheless, even the largest dataset (Crop3D in 2024 (Zhu et al., 2024)) to date only approaches the scale of ScanNet (Dai et al., 2017), which was introduced in 2017, and still remains smaller. The seven-year lag in data scale underscores a persistent gap between plant-specific resources and general 3D vision datasets. Furthermore, Crop3D does not provide instancelevel organ annotations, which are essential but extremely labor-intensive and costly to generate. To achieve the full potential of 3D computer vision in 3D plant phenotyping, additional datasets of larger scale and richer annotations are urgently needed. At the same time, the availability of these limited yet emerging datasets presents both challenges and unique opportunities for advancing the algorithmic and computational components of the data-algorithm-computing triangle.

3. Deep learning-based methods for 3D point cloud segmentation

Accurate segmentation of plant point clouds is a crucial prerequisite for 3D plant characterization. In this section, we reviewed representative methods for both point cloud semantic and instance segmentation and their applications for plant phenotyping.

3.1. Semantic segmentation

Semantic segmentation aims to assign a semantic class label to every point in a 3D point cloud. For plant phenotyping at the organ level, this process categorizes points based on their corresponding organ types that are defined by plant biology. In general, semantic segmentation can be divided into point-based, voxel-based, and hybrid methods.

3.1.1. Point-based methods

Point-based methods directly operate on unstructured point clouds. The seminal work of point-based methods is

Table 1Summary of the current available datasets, the datasets marked with * were used in the benchmarks. The number of data samples refer to the samples that are annotated. For simulated datasets, the number of data samples are usually customized by the users.

	Dataset	Year	Plant type	Number of samples	Features	Annotations	Imaging
Real-world	Eschikon Plant Stress (Khanna et al., 2019)	2019	Sugar beet crop	16	X, Y, Z, R, G, B, 25 narrow band reflectance values	\	Multi-modalities
	ROES-X (Dutağacı et al., 2020)	2020	Rose	11	X, Y, Z	Sem.	X-ray scanning
	*Pheno4D (Schunck et al., 2021)	2020	Maize; Tomato	126	X, Y, Z	Sem., Inst.	Laser scanning
	PFuji-Size (Gené-Mola et al., 2021)	2021	Apple tree; Apple	6 (Apple tree); 640 (Apple)	X, Y, Z, R, G, B	Sem., Inst. (Apple)	SfM-MVS
	Panicle3D (Gong et al., 2021)	2021	Rice	200	X, Y, Z	Sem.	Structured light
	*HR3D (Conn et al., 2017a)	2022	Tomato; Sorghum; Tobacco	546	X, Y, Z	Sem., Inst.	Laser scanning
	Cotton3D (Saeed et al., 2023)	2023	Cotton	30	X, Y, Z, R, G, B	Sem., Inst.	Laser scanning (TLS)
	*SoybeanMVS (Sun et al., 2023b)	2023	Soybean	102	X, Y, Z, R, G, B	Sem., Inst.	MVS
	*SYAU-Maize (Yang et al., 2024)	2024	Maize	428	X, Y, Z	Sem., Inst.	Laser scanning (HLS)
	PLANesT-3D (Mertoğlu et al., 2023)	2024	Pepper; Rose; Ribes	34	X, Y, Z, R, G, B	Sem., Inst.	SfM-MVS
	Crop3D (Zhu et al., 2024)	2024	Cotton; Maize; Potato; Wheat; Cabbage, etc.	1230	X, Y, Z, R, G, B	Sem., Inst. (Plant- level)	Multi-modalities
	*COS (Du et al., 2024; Qiu et al., 2024a)	2025		98	X, Y, Z	Sem., Inst.	Laser scanning (TLS)
Synthetic	Lpy-Arabidopsis&Lilac (Chaudhury et al., 2020)	2020	Arabidopsis; Lilac		- X, Y, Z, R, G, B	Sem., Inst.	Synthetic
	Simulated roses (Turgut et al., 2022)	2022	Rose	\	X, Y, Z	Sem., Inst.	Synthetic
	LTree-Panel (Qiu et al., 2025)	2025	Apple tree	\	X, Y, Z	Sem., Inst.	Synthetic

 Table 2

 Representative 3D segmentation datasets across different domains. For certain indoor and urban scene datasets where the total number of samples is not explicitly reported, we provide the total spatial coverage as described in their original publications instead.

	Dataset	Year	Total samples/Spatial size
Indoor scene seg.	S3DIS (Armeni et al., 2016)	2016	6020 <i>m</i> ²
	ScanNet (Dai et al., 2017)	2017	1513
Object part seg.	ShapeNet (Yi et al., 2016) PartNet (Mo et al., 2019) Fusion 360 Gallery (Lambourne et al., 2021)	2019	31963 26671 35858
Roadway scene seg.	SemanticKITTI (Behley et al., 2021)	2019	43552
	KITTI360 (Liao et al., 2021)	2021	80000
Urban scene seg.	Semantic3D (Hackel et al., 2017)	2017	30 TLS scans (up to 1.15 km²)
	DublinCity (Zolanvari et al., 2019)	2019	2.0 km²
	SensatUrban (Hu et al., 2021)	2020	7.64 km²
	DALES (Varney et al., 2020)	2020	10 km²
	CUS3D (Gao et al., 2024)	2023	2.85 km²

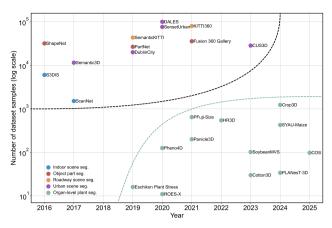


Figure 2: Data size over publication year of publicly available datasets for both general 3D computer vision (top-left region) and 3D plant phenotyping (bottom-right region). For datasets that only report spatial coverage, we approximated total samples using partition blocks of $1m \times 1m$ for indoor scenes and $10m \times 10m$ for urban scenes as suggested in (Qi et al., 2017a; Han et al., 2021).

PointNet (Qi et al., 2017a). PointNet processes each point independently using a series of shared multi-layer perceptrons (MLPs) to extract features. The most prominent contribution of PointNet is to combine features from individual points as a global feature vector through symmetric functions (e.g., max pooling) that preserve permutation invariance for unordered points in a point cloud. The resultant global feature vector can be used for successive point cloud classification and segmentation. While PointNet has inspired the use of deep learning directly on point clouds, it has limitations in learning local geometric feature and spatial relationship among points, as each point is encoded individually. Successive studies have attempted to addressing these limitations for resolving detailed patterns and processing complex scenes.

Neighboring feature aggregation: A straightforward extension is to encode features from spatially neighboring points in the metric space, yielding a feature vector that captures both individual point characteristics and the structure of their local region and/or across spatial scales. Point clustering and feature aggregation strategies are the key factors influencing model performance, and extensive studies have investigated diverse options such as ball-query, K nearest neighboring (KNN) search, orientation-specific search, and K-means clustering for point grouping (Qi et al., 2017b; Jiang et al., 2018; Engelmann et al., 2018; Hu et al., 2020) and various pooling or weighted combination for feature aggregation (Shen et al., 2018; Zhao et al., 2019; Wu et al., 2019). Point grouping can also be achieved through transforming raw points into **graph representations** (e.g., dynamic graphs, superpoint graphs) which capture spatial relationship among points during the construction of the graph. Subsequently, graph theory and processing operations can be used to extract features describing both individual points and their contextual information (Wang et al., 2019a,b; Landrieu and Simonovsky, 2018; Landrieu and Boussaha, 2019).

Point convolution: An alternative approach is to extend convolution operations to directly process raw, unordered points. Point clouds can be considered as sparse sampling from a continuous space (Wang et al., 2018b), presenting challenges to design convolution operations with satisfactory computation and memory use efficiency (Wu et al., 2019; Thomas et al., 2019; Baa et al., 2020) or permutation invariance (Xu et al., 2021). A viable option is to reparameterize convolution operations, so these operations can be analytically traceable on unordered points. A notable work is deep parametric continuous convolution in which a MLP is used as the function approximator to estimate continuous convolution values at an arbitrary point sampled from a continuous space, namely, a point in the point cloud (Wang et al., 2018b; Hornik, 1991). Another option is to use positional information to adaptively associate points with kernel weights to reduce the computational complexity. For instance, position adaptive convolution (PAConv) predefines a set of weight matrices and uses an MLP to calculate coefficients of weight matrices at a point based on the relative distances between that point and neighboring ones (Xu et al., 2021). This process dynamically creates convolution kernels adapted to point position without computationally expensive one-to-one mapping.

In summary, the major advantage of point-based methods lies in their ability to operate directly on raw point cloud data, thereby preserving fine-grained shape information in the final result. Owing to this advantage, many studies have investigated point-based neural networks for plant point cloud segmentation (Li et al., 2022b; Dutağacı et al., 2020; Turgut et al., 2022; Li et al., 2025a, 2022a; Yang et al., 2024; Patel et al., 2023). Point-based methods still encounter computational challenges, particularly regarding GPU memory limitations, when processing high-resolution and large-scale dense point clouds. Although downsampling can effectively reduce input data volume and, consequently, computational costs, it introduces the critical trade-off between reducing computational complexity and preserving essential information. Excessive downsampling risks the elimination of many plant organs, which are crucial for accurate organlevel plant phenotyping. Therefore, specialized downsampling techniques tailored to this domain are necessary (Li et al., 2024b, 2023). To circumvent this trade-off, sliding window-based inference techniques have been used. In this approach, the point cloud of a scene or object is partitioned into smaller patches, enabling the network to process subsets of points without directly addressing the balance between resolution and computational load. However, this strategy inherently restricts the network's total receptive field and thus its ability to capture global point relationships.

3.1.2. Voxel-based methods

Voxelization converts raw, unordered points into gridded voxels, enabling the use of discrete convolution operations. 3D convolutional neural network (3D CNNs) are a direct choice and provide hierarchical feature extraction through

a stack of convolution layers that preserve both local features in shallow layers and global features in deeper layers. This feature of 3D CNNs has proven to be crucial for segmentation tasks (Oi et al., 2017b; Long et al., 2015). Early attempts have explored dense 3D CNN structure that applies 3D convolution operations across the entire dense voxel grids (Huang and You, 2016; Tchapmi et al., 2017). The performance of dense 3D CNNs highly relies on the resolution of the voxelization process. The memory usage grows at least cubically for storing dense 3D voxels and calculating 3D convolution (Maturana and Scherer, 2015), requiring a trade-off between computation cost and processing resolution. This trade-off is non-trivial because plant point clouds must have sufficient spatial resolution to keep information of certain types of plant organ (e.g., stems or fruits) for organ-level plant phenotyping (Jin et al., 2020; Li et al., 2022b). In some cases, such a trade-off may not even be available, so dense 3D CNNs have been less used in successive studies.

Since many voxels are empty (i.e., no point in a voxel) in high-resolution voxel grids, sparse convolution operation has been proposed to exploit this characteristic and perform computation only on non-empty (also known as active) voxels and their neighbors, which drastically reduces computational complexity and memory usage yet avoids the need of spatial resolution loss (Graham, 2015; Graham et al., 2018). An important development is the submanifold sparse convolution (SSC) operation that shares the list of active points between the input and output to regulate the spread of point activation after convolution. SSC then only computes active input points to avoid unnecessary resource uses compared to dense convolution. Integrating SSC and strided sparse convolution with the U-Net like architecture (Çiçek et al., 2016) forms a network that is capable of handling high-resolution point clouds with leading performance. More recently, sparse convolution operations have been widely adopted to construct neural networks for 3D point cloud segmentation because of the development of specialized libraries such as SpConv (Contributors, 2022), Minkowski Engine (Choy et al., 2019), and TorchSparse series (Tang et al., 2022, 2023b). These libraries provide highly optimized implementations of sparse convolution operations, making the training and deployment of deep 3D sparse CNNs much more feasible.

Sparse convolution operations are very suitable for organ-level plant phenotyping because these operations can offer both computation efficiency for large volumetric data points and capability of extracting features across multiple scales through a stack of operations (Luo et al., 2023; Qiu et al., 2025; Li and Su, 2025; Ge et al., 2025; Marks et al., 2024). Determining the proper step size of the voxelization process remains challenging. If the resolution is too coarse, details of small plant organs (e.g., thin branches, stems) can be smoothed or even diminished. Conversely, if the resolution is too fine, the number of active voxels can still become very large, increasing computation costs even with sparse convolutions. Since plant organ size varies at different

plant growth stages and among different plant species, it is hard to suggest common values and worthy of further investigation.

3.1.3. Hybrid methods

Hybrid methods include methods that combine point clouds with other data representations (e.g., RGB-D images, voxels) (Guo et al., 2020). Specifically, in this review, we refer hybrid methods to those that leverage the advantages of point-based and voxel-based representations (i.e., combine point and voxel representations in data processing).

The essence of these hybrid methods is to leverage the fine-grained details preserved from light-weight point-based feature extractors (e.g., MLPs) while benefiting from the high capability for neighboring feature learning and the structured nature of voxel-based convolutions. These two streams of information are subsequently fused to generate a comprehensive feature set for segmentation. Representative network includes point-voxel CNN (PVCNN) (Liu et al., 2019) and its successor sparse point-voxel convolution (SPVConv) that integrates sparse convolution to extend its segmentation performance and capability of handling large 3D scenes (Tang et al., 2020). These hybrid approaches are gaining popularity for plant point cloud segmentation (Cui et al., 2025).

3.2. Instance segmentation

Instance segmentation extends semantic segmentation and further identifies individual instances of the same class. Based on the order of semantic and instance identification, instance segmentation can be categorized into three strategies: proposal-based, grouping-based, and transformer-based.

3.2.1. Proposal-based methods

Proposal-based 3D instance segmentation methods, inspired by their 2D counterparts (He et al., 2017; Wang et al., 2020a,b), use a top-down strategy that generates potential object proposals (i.e., instance bounding boxes) and then refines these proposals to predict final instance masks (Yang et al., 2019; Yi et al., 2019; Sun et al., 2023a; Kolodiazhnyi et al., 2024a). While this strategy is intuitive and has demonstrated great success in 2D instance segmentation, it did not achieve expected performance for processing 3D point clouds (Chen et al., 2021; Jiang et al., 2020; Vu et al., 2022, 2024; Kolodiazhnyi et al., 2024a). A major bottleneck is the precision of proposal generation which influences feature extraction capacity (Sun et al., 2023a). In 2D images, proposals can have slight offset from objects of interest but still contain sufficient information for successive feature extraction. In 3D point clouds, points are collected only from object surface and usually cannot represent the inner structure of an object. Therefore, subtle positional shift of proposals (i.e., 3D bounding box) may result in losing a considerable amount object points, presenting significant challenges to feature extraction and subsequent segmentation. This challenge is originated from the nature of data collection of point clouds, limiting the development and

application of proposal-based methods. Little or no information has been reported to use proposal-based methods for plant point cloud instance segmentation. As a result, we did not provide further review on this strategy.

3.2.2. Grouping-based methods

Grouping-based methods usually build upon a bottomup strategy that extracts features and predict semantic labels at the point level and then groups points into individual instances. There are two key factors influencing the performance of grouping-based methods: point-wide semantic prediction accuracy and grouping strategy. Advances in semantic segmentation are reviewed in Section 3.1, so we focus on the improvement of grouping strategy in this section.

While simple clustering algorithms can be used to group semantic points, recent studies have investigated semantic latent embeddings (Tong et al., 2020; He et al., 2020, 2021) or graph representations (Liang et al., 2021; Engelmann et al., 2020; Han et al., 2020) to enhance feature richness and representativeness for improved grouping performance. Among recent efforts, PointGroup plays a critical role in advancing the grouping-based 3D instance segmentation (Jiang et al., 2020). The key of PointGroup is the dualset point features compromising common point features extracted from MLPs and offset vectors of individual points relative to instance centroids. The common point features are useful to predict semantic labels but may mis-assign instance identification for each point, whereas the offset vectors are good at grouping points into individual instances. Collective utilization of the dual-set features leverages complementary strengths of each feature set. This strategy is particularly promising for handling complex plant point clouds, as it excels at disentangling tightly packed organ instances within individual plants (Du et al., 2023; Li and Su, 2025; Li et al., 2025b). Building upon PointGroup, SoftGroup (Vu et al., 2022, 2024) was proposed to address point grouping errors caused by hard semantic prediction which is a common challenge in the bottom-up strategy of grouping-based methods. SoftGroup enables each point to be associated with multiple semantic scores rather than a single class label, transforming semantic labeling from hard classification to soft probability estimation. This change mitigates the error propagation from the semantic identification step to the grouping step in instance segmentation.

Grouping-based methods have two general limitations. One is that the point grouping step relies on the semantic identification step, lacking direct instance-level supervision during training and therefore demanding a post-processing refinement (Sun et al., 2022). Another is that grouping-based methods usually have many hyper-parameters that significantly influence model performance yet need careful tuning in different datasets, hindering the generalizability of grouping-based methods across diverse applications (Kolodiazhnyi et al., 2024a).

3.2.3. Transformer-based methods

In the past two years, transformer-based methods have been extensively studied and quickly become the leading analysis strategy for 3D instance segmentation. Transformerbased methods take the advantage of attention mechanism to unify feature learning for joint optimization of semantic prediction and instance identification without separating and then combine results from the semantic and instance tasks. Mask3D (Schult et al., 2023) is one of the pioneering transformer-based models and integrates 3D sparse convolution U-Net (Choy et al., 2019) as feature encoder with a transformer decoder consisting of masked and sampled attentions (Cheng et al., 2022). The sparse U-Net extracts voxel feature maps at multiple spatial scales that are fed into the transformer decoder where each query represents one instance in the scene. In the decoder, each query is cross-attended with the multiscale voxel feature maps and self-attended with other queries to enforce one query per instance.

Around the same time, superpoint transformer (SP-Former) was proposed to combine 3D sparse U-Net and transformer decoder as a unified end-to-end model for 3D instance segmentation (Sun et al., 2022). SPFormer is different from Mask3D in the model architecture designing. SPFormer explicitly integrates bottom-up and top-down strategies into the unified model architecture. In the encoding stage, in addition to feature maps from 3D sparse U-Net, SPFormer groups raw points into superpoints and applies superpoint pooling to merge raw point features and superpoint features. This process is considered to provide the bottom-up grouping information. In the decoding stage, the transformer decoder cross-attends the superpoint features to generate instance proposals, which is the top-down instance proposal information. Both Mask3D and SPFormer demonstrated significant improvements for 3D instance segmentation, but SPFormer could be a better choice for analyzing largescale point clouds because of computational efficiency by superpoint (Landrieu and Simonovsky, 2018).

As of writing this review, OneFormer3D (Kolodiazhnyi et al., 2024b) achieves the leading performance for 3D instance segmentation. While maintaining fast inference speed, OneFormer3D further streamlines the integration of feature maps from sparse convolution network and query decoding in transformer decoders by parallel training of semantic and instance queries and a cost-effective query selection. As a result, Oneformer3D solves semantic, instance, and panoptic segmentation jointly.

In summary, transformer-based decoders enable the direct integration of feature learning from input point clouds or voxels into semantic prediction and instance masking. This process minimizes or even avoids subjective design choices and hyperparameter tuning of hand-crafted top-down (proposal-based methods) or bottom-up (grouping-based methods) strategies for instance differentiation. Further, such a streamlined integration would allow joint optimization of multiple 3D segmentation tasks, which usually

provide a performance boost in practice. Given these advantages, transformer-based methods have been investigated in 3D plant phenotyping in very recent years (Qiu et al., 2025; Du et al., 2024).

4. Plant segmentation studio

In addition to the qualitative review in Section 2 and Section 3, a quantitative review would be valuable to objectively identify common challenges of 3D point cloud segmentation for organ-level plant phenotyping. The first barrier for conducting a quantitative review for 3D plant phenotyping is the lack of a unified framework that can standardize data management and streamline processing pipeline for comparative studies. In general computer vision, such frameworks like MMDetection, MMDetection3D (Contributors, 2020), and Detectron2 have enabled the research community to quickly identify issues or recognize significant improvements for substantial advancement. Inspired by this, we developed Plant Segmentation Studio (PSS) as the first attempt to address this considerable gap and used PSS to perform computational experiments for a quantitative review on 3D plant segmentation for organ-level plant phenotyping.

PSS builds upon MMDetection3D that is a modular framework for a wide range of 3D computer vision tasks including 3D semantic segmentation and detection. Compared with MMDetection3D, PSS is tailored to 3D plant phenotyping by customizing dataset preparation, including representative modules and algorithms for 3D segmentation, and streamlining the configuration of analysis pipelines.

4.1. Dataset preparation

MMDetection3D typically uses a comprehensive datasetspecific pipeline optimized for widely adopted benchmarks, where built-in metadata, such as the mapping between semantic meaning to annotations, and training-validation splits, are hardcoded for efficient data handling and results review. While beneficial for standard benchmark datasets, this approach presents less flexibility for customized applications in two ways:

- Requiring repetitive manual configuration for newly added datasets.
- ii) Inflexibility when adjusting dataset splits.

PSS collects and integrates several popular plant point cloud datasets, providing detailed meta information, and implements a simplified data preparation pipeline to convert these datasets into a standardized format. It features a unified, intuitive JSON-based configuration system. Users only need to:

- i) Structure their point cloud data in a straightforward intermediate format (e.g., txt, csv, ply point clouds).
- ii) Specify essential metadata within a single JSON file, as shown in Fig. 3(a) to provide a global semantic-annotations mapping for both semantic and instance segmentation.

This approach enables an intuitive access to user-customized data and significantly lowers the workload associated with data conversion and standardization.

4.2. Representative 3D segmentation algorithms

The default workflow of MMDetection3D emphasizes 3D object detection, which does not directly support instance segmentation, a critical task for segmentation-based 3D plant phenotyping. To overcome this algorithmic gap, PSS incorporates two representative instance segmentation networks specifically optimized to be compatible with the simplified dataset structure. Specifically, PSS incorporates two advanced segmentation networks: OneFormer3D (Kolodiazhnyi et al., 2024b), which uses learnable queries to simultaneously perform semantic and instance segmentation; and SoftGroup (Vu et al., 2022), which employs grouping algorithms combined with subsequent refinement steps for instance segmentation. Additionally, a baseline voxel-based method, SCUNet (Section 5.1.2), is also implemented for benchmarking purposes.

Given that hyperparameter tuning across various plant species datasets can be tedious, PSS also provides automated tools for inferring essential network hyperparameters directly from user-supplied datasets. Furthermore, all newly integrated segmentation networks can seamlessly interact with existing semantic segmentation backbones provided by MMDetection3D, enabling researchers to efficiently create customized algorithms.

4.3. Streamlined inference pipelines

MMDetection3D's extensive flexibility in network support and customizable design results in complex computational workflows due to intricate module inheritance relationships. Domain scientists in plant phenotyping and agriculture often lack the computer vision expertise required to effectively run these networks and review the results.

To enhance the usability, except for the efforts in Section 4.1. PSS provides a unified inference pipeline supporting all included segmentation networks. This standardized inference interface ensures comprehensive and consistent processing of segmentation outputs across different network architectures. Specifically, for instance segmentation, PSS applies the appropriate inference logic based on whether the model is transformer-based or grouping-based and provides detailed inference outputs (e.g., shifted coordinates for grouping-based methods. By integrating simplified processes from initial data preparation through final inference within an intuitive workflow, PSS significantly lowers technical barriers. As a result, researchers can efficiently achieve reproducible results, perform systematic algorithm comparisons, and accelerate the development and validation of novel segmentation methods suitable for diverse 3D plant phenotyping applications.

Overall, PSS aims to address existing gaps in data handling, algorithm integration, and computational workflow usability, reducing required expertise and facilitating broader adoption of deep learning-based segmentation approaches among domain scientists. While this study alone

Table 3Summary of benchmark datasets. HR3D and Pheno4D, which contains multiple species (Table 1), are jointly trained and tested in all experiments.

Dataset	Source	Train	Test	PSS annotations
COS	(Du et al., 2024; Qiu et al., 2024a)	72	26	0:trunk, 1:branch
HR3D	(Conn et al., 2017a,b)	377	169	0:stem, 1: leaf
SYAU-Maize	(Yang et al., 2024)	349	79	0:stem, 1: leaf
Pheno4D	(Schunck et al., 2021)	90	36	0:ground, 1:stem, 2:leaf
SoybeanMVS	(Sun et al., 2023b)	65	37	0:mainstem, 1:stem, 2:leaf

does not yet fully establish an integrated data-algorithm-computing nexus, we envision it as a foundational contribution—a step toward enabling future innovations and fostering continued advancement in the field of plant phenotyping.

5. Benchmarks

5.1. Methods

5.1.1. Benchmark dataset statistics

The split and annotations for 5 benchmark datasets used through all experiments are listed in Table 3.

Processing plant point cloud datasets for DL-based segmentation poses several challenges due to the diverse points and organs distributions, and the sensitivity of morphological representation to point cloud resolution differences across datasets. As shown in Fig. 4, the number of points per semantic class varies considerably between datasets. Pheno4D and SoybeanMVS offer the highest point densities per sample, often ranging from 10⁵ to 10⁶, providing rich detail across multiple organ classes. In contrast, HR3D and SYAU-Maize contain far fewer points, which may limit their ability to capture fine-grained, organ-level features. Additionally, COS exhibits a highly imbalanced trunk-to-branch class distribution, potentially biasing feature learning during network training.

Fig. 5 illustrates the variation in annotated organ instance counts across datasets. HR3D, SYAU-Maize, and Pheno4D include relatively few annotated organ instances (typically fewer than 20 per sample), whereas SoybeanMVS provides a broader range, supporting richer instance-level variability.

A common challenge across all plant point cloud datasets is the trade-off between input resolution and morphological completeness. Plant morphology comprises thin, elongated, and intricately connected structures that are highly sensitive to data resolution changes. However, deep learning models, whether point-based or voxel-based, require resolution reduction to manage memory and computational constraints. Techniques such as point downsampling or strided convolution for hierarchical feature learning can significantly degrade geometric fidelity, especially in high-resolution datasets, leading to the loss of critical fine-grained information necessary for accurate segmentation (Fig. 6).

To address these limitations, resolution-aware strategies are essential. In point-based approaches, block-wise down-sampling within constrained regions helps preserve structural details, and sliding-window inference during prediction

further improves coverage. For voxel-based methods, integrating skip connections between multiple voxel resolutions is crucial for capturing both coarse and fine features.

5.1.2. Benchmark models

For semantic segmentation tasks, encoder—decoder architectures have proven highly effective at capturing large receptive fields through sequential downsampling and upsampling operations (Xu et al., 2021). Deep neural networks built on this structure typically achieve a balance between computational efficiency and segmentation accuracy. Most grouping-based or transformer—based instance segmentation networks can be regarded as extensions of semantic segmentation models, incorporating an additional instance head on top of the semantic head.

In this study, we benchmark 6 semantic segmentation networks and 6 instance segmentation networks (Fig. 3). The semantic segmentation baselines include PointNet++, DGCNN, PAConv, SCUNet, MinkUNet, and SPVConv. For instance segmentation, OneFormer3D and SoftGroup are established baselines, while 4 additional models are new implementations that combine different semantic and instance heads (Table 4). The details of these networks are as follows:

PointNet++ enhances the original PointNet architecture by introducing a hierarchical set abstraction (SA) structure to capture local geometric features. It consists of multiple SA layers as the encoder and feature propagation (FP) layers as the decoder. Each SA layer comprises three components: a sampling layer, a grouping layer, and a PointNet block. Point resolution is progressively reduced through farthest point sampling, while local features are aggregated via a ball query of neighboring points. The decoder then restores the original resolution through interpolation across FP layers, allowing the network to efficiently capture both local and global structure.

DGCNN introduces EdgeConv, an operation that dynamically constructs local neighborhood graphs. EdgeConv explicitly models relationships between a point and its knearest neighbors (kNN) and aggregates features through max-pooling to produce robust global descriptors. Unlike static graph approaches, DGCNN recomputes graph structures in the feature space at each layer, enabling the network to capture increasingly rich semantic relationships and geometric detail across all points.

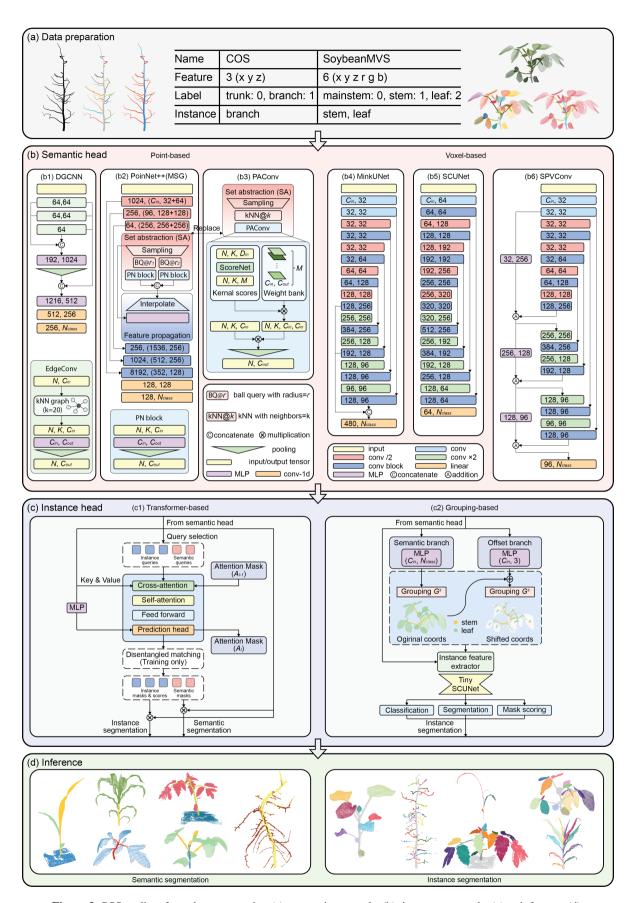


Figure 3: PSS outline, from data preparation (a), semantic networks (b), instance networks (c) to inference (d).

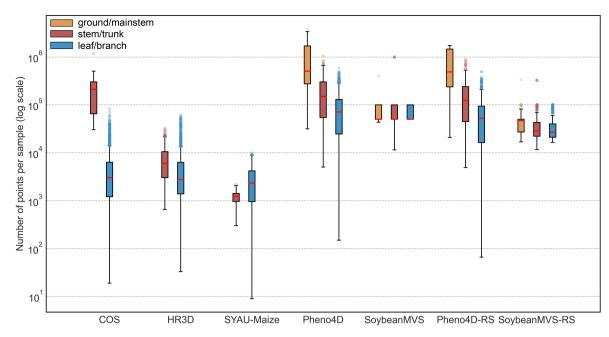


Figure 4: Distribution of number of points per sample of different semantic classes across seven datasets. Due to the substantial size of the Pheno4D and SoybeanMVS datasets, we created random-sampled subsets (denoted as Pheno4D-RS and SoybeanMVS-RS), reserving the original organ instances statistics (Fig. 5), to facilitate instance-level evaluations while reserve the maintaining computational efficiency.

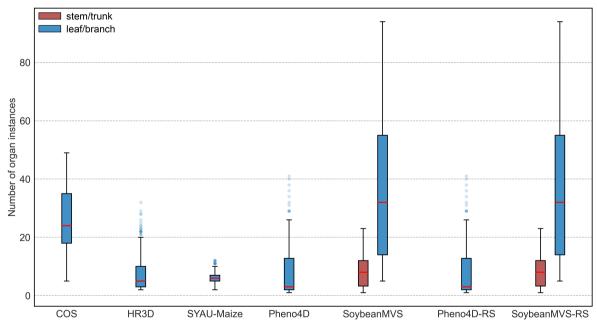


Figure 5: Distribution of number of organ instances across the seven datasets. The number of certain organs of 0 or 1 in a dataset are ignored for illustration. (e.g., trunk for COS dataset).

PAConv introduces a position-adaptive convolution for point clouds by dynamically assembling convolutional kernels. Instead of fixed kernels, PAConv generates kernels from a learnable Weight Bank based on the relative positions of points, with weights predicted by ScoreNet. This flexible kernel assembly improves segmentation performance on irregular point clouds and can be integrated into various

backbones. In our benchmarks, PAConv replaces all MLP layers in a PointNet++ backbone, and we refer to this configuration simply as "PAConv."

Sparse convolution U-Net (SCUNet) extends the 3D U-Net architecture with sparse convolution operations to

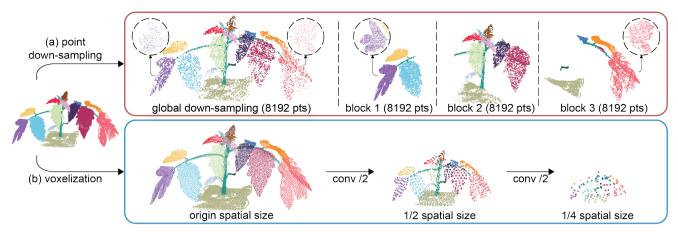


Figure 6: (a) For point-based methods, point downsampling is necessary to reduce computational cost (downsampling to 8192 points in illustration). However, global downsampling can lead to severe loss of morphological detail. To alleviate this, block-wise downsampling within smaller spatial regions is employed to preserve more information. (b) For voxel-based methods, voxelization transforms point clouds into structured 3D grids. As the network deepens, the resolution of intermediate feature maps decreases significantly due to strided convolutions (stride=2 in illustration). In such cases, skip connections across multiple resolutions are critical for retaining fine-grained morphological information throughout voxel-based network.

address the sparsity of 3D point clouds. Unlike dense voxelization methods subject to high memory and computational costs, SCUNet uses submanifold and sparse convolutions to process only occupied voxels efficiently. The encoder gradually aggregates multi-scale features, while the decoder restores spatial resolution through transposed sparse convolutions and skip connections. This design improves computational efficiency and accuracy. Currently, there are three widely-used backends: SpConv (Contributors, 2022), Minkowski Engine (Choy et al., 2019), and TorchSparse (Tang et al., 2022, 2023a,b) support sparse convolutions. In benchmarks, SCUNet is implemented using SpConv following OneFormer3D's configurations.

MinkUnet builds upon SCUNet by incorporating skip concatenation between encoder and decoder layers to fuse fine-grained spatial details with high-level semantic features. Our implementation uses TorchSparse, leveraging its optimizations for sparse tensor operations. Detailed backend comparisons are available in (Contributors, 2020).

Sparse point-voxel convolution (SPVConv) is a hybrid framework combining point-based and voxel-based representations. A dual-branch design enables point-based modules to capture fine-grained details while voxel-based modules, structured as a sparse convolutional U-Net, provide a broad receptive field and contextual information. Feature fusion occurs at multiple stages, enabling SPVConv to leverage the strengths of both representations. We use TorchSparse for implementation in benchmarks.

OneFormer3D integrates voxel features with learnable semantic and instance queries processed by six sequential transformer decoders. Each decoder applies cross-attention between queries and voxel features, alongside self-attention among queries. Attention masks are progressively refined to spatially constrain cross-attention of queries to more

specific voxel regions for distinguishing different semantics and instances.

SoftGroup employs a semantic branch to predict point-level semantic scores and an offset branch to estimate vectors shifting points toward their respective instance centers. Grouping is performed on these dual coordinates using a ball query, guided by semantic scores. In the refinement stage, a lightweight U-Net predicts instance class labels, masks, and confidence scores to produce the final instance segmentation results.

5.1.3. Synthetic training data generation

Based on the discussion of synthetic 3D plant data generation in Section 2.2 and their potential for sim2real learning, this section focuses on two representative implementations of PM-based and augmentation-based pipelines applied to COS datasets:

L-TreeGen comprises two key components: (i) a tree generation (TG) module based on inverse procedural modeling to create biologically plausible tree meshes, and (ii) a virtual laser scanning (VLS) module to replicate the sensing characteristics of laser scanners used in the field. The TG module operates in two steps. First, trunk and primary branch morphologies are interpolated from key statistics (e.g., trunk height, skeleton structure, branch radius) derived from real tree point clouds. Next, higher-order branches are hierarchically scaled and attached to primary branches to create realistic, complex branch structures. Biological constraints, including tapering effects (progressive thinning of trunks and branches) and collision detection between organs, are incorporated to ensure morphological plausibility. The VLS module, implemented using Helios++ (Winiwarter et al., 2022), enables configurable sensor parameters to simulate acquisition imperfections such as noise, occlusion, and

Table 4
Summary of semantic and instance segmentation networks in the benchmark. For simplicity, we name the 4 new implemented networks according to their semantic and instance heads combinations. E.g., Mink-SG (MinkUnet with SoftGroup grouping), SPVConv-SG (SPVConv with SoftGroup grouping), MinkFormer (MinkUnet with OneFormer3D query decoder), and SPVFormer (SPVConv with OneFormer3D query decoder). Notably, for SPVConv, its point-branch use the points after quantization, therefore, we consider it both hybrid and voxel-based methods.

		Representation	Encoder	Decoder					
Semantic	PointNet++	Point-based	Set abstractions (w/ MLP)	Feature propagation					
	DGCNN	Point/Graph-based	Edge convolution	MLP					
	PAConv	Point-based	Set abstractions (w/ position adaptive convolution)	Feature propagation					
	SCUNet	Voxel-based	SCUNet (w/ SpConv backend)						
	MinkUnet	Voxel-based	SCUNet (w/ Torchsparse backend, skip concatenation)						
	SPVConv	Hybrid/Voxel-based	SCUNet (w/ Torchsparse backend, Point-wise MLP, skip addition)						
			Semantic head	Instance head					
Instance	SoftGroup	Voxel-based	SCUNet (Vu et al., 2022)	Grouping					
	Mink-SG	Voxel-based	MinkUnet	Grouping					
	SPVConv-SG	Hybrid	SPVConv	Grouping					
	OneFormer3D	Voxel-based	SCUNet (Kolodiazhnyi et al., 2024b)	Transformer decoder					
	MinkFormer	Voxel-based	MinkUnet	Transformer decoder					
	SPVFormer	Hybrid/Voxel-based	SPVConv	Transformer decoder					

variations in resolution, angle, and scanner positioning. L-TreeGen not only produces biologically realistic tree models but also replicates sensor artifacts, generating imperfect training data designed to improve neural network generalization to real-world conditions.

Deformation uses physics-based elastic deformation to deform plant structures through simulated external forces to generate new plant point clouds. This process has two main steps. First, the original plant point cloud is voxelized, and physical properties (e.g., Young's modulus, Poisson's ratio) are assigned to voxels representing different organs. Second, external forces of controlled magnitude, direction, and application positions (i.e., voxel vertices) are applied. Throughout the whole process, elastic deformation mechanics ensure accurate force transmission and preserve organ topology, minimizing artifacts. By systematically changing applied forces, deformation enhances dataset variability while introducing fewer distortions compared to brute-force augmentation techniques such as scaling, rotation, flipping, or jittering. Following the strategy in (Yang et al., 2024), we conducted deformation experiments using a voxel size of 0.001 and external forces ranging from -5 to 5 N along the X, Y, and Z axes.

The evaluation of L-TreeGen and deformation provides insight into the practical benefits and limitations of each approach. Both demonstrate effective strategies for reducing annotation burdens and improving model generalization. PM-based methods emphasize biological realism but involve higher complexity, whereas augmentation-based methods focus on feature diversity and scalability, often at the cost of reduced biological fidelity.

5.2. Experiments

The experiments are divided into 3 parts. First, we benchmark the performance of 6 semantic segmentation networks. Next, we select 2 representative semantic heads and 2 instance heads to construct 4 new instance networks, which are evaluated alongside the original SoftGroup and OneFormer3D. Finally, we use the best-performing instance network to investigate the effectiveness of synthetic data for sim2real learning. All experiments were conducted in PSS.

5.2.1. Data preparation for semantic and instance segmentation

All 5 benchmark datasets (Table 3) are used to evaluate the performance of semantic and instance segmentation networks. During training, each dataset is augmented on-the-fly to ensure a sufficient training set size. Specifically, random sampling is applied for point-based semantic segmentation, while flipping and scaling are used for voxel-based semantic segmentation. These augmentation methods are chosen to enable each network to reach its maximum performance potential.

5.2.2. Data preparation for sim2real learning

Using the established L-TreeGen and deformation pipelines, we conducted 3 experiments on the COS dataset to assess the potential of synthetic data for sim2real learning and to determine which synthetic data generation strategy is most suitable for different segmentation tasks. The training and testing splits are identical to those in the semantic and instance segmentation benchmarks (72 training and 26 testing samples). To ensure balanced representation, training samples were equally selected from two orchards (36 from

each), as the trees exhibit different morphological characteristics in each orchard. This balance was also maintained when selecting base trees for synthetic data generation.

For clarity, we define the real-world trees used to generate synthetic data as **base trees**, with the number of base trees in a subset denoted as K_b . Unless noted, each subset of base trees was used to generate 150 synthetic trees for training. We categorize the experiment setups as follows:

- **0-shot**: Training only on synthetic data, followed by direct testing on real-world data.
- K_b-shot: Pre-training with synthetic data, fine-tuning with K_b base trees, and testing on real-world data.
- Vanilla (Baseline): Training exclusively on all realworld data without synthetic data.

The three experiments are designed as follows:

- Robustness of L-TreeGen and deformation in 0-shot segmentation: When the number of base trees is small, their composition can strongly influence the geometric feature distribution of the generated synthetic trees, potentially introducing learning bias. To investigate this effect across different synthetic data generation methods, we randomly sampled six base trees ($K_b = 6$, where 3 from each orchard) without replacement from the training set of 72 trees to form 12 non-overlapping subsets (12 folds). We then evaluated the 0-shot performance for each subset.
- Segmentation performance with different base tree sizes for synthetic data generation: The 12 subsets from the above experiment were ranked by instance segmentation performance (using AP metric). We aggregated base trees from the top-performing folds to create larger subsets with $K_b = 12$, 18, and 24, representing upper-bound subsets. Similarly, subsets were formed from the lowest-ranked folds to establish lower-bound subsets. We evaluated both 0-shot and K_b -shot performance for all subsets.
- Resolution comparison of L-TreeGen: More realistic synthetic data, incorporating sensor imperfections, may improve network generalization on real-world data. In this experiment, both TG and VLS modules of L-TreeGen were used to generate synthetic trees at three sensor angular resolutions: 0.3, 0.06, and 0.03 degrees (denoted as VLS03, VLS006, and VLS003). Lower values indicate higher point cloud resolution. Using the upper-bound subset with K_b = 24, we compared 0-shot and K_b-shot performance to assess the effect of resolution and establish the best achievable performance of synthetic data for sim2real learning relative to the vanilla setup.

Detailed data preparation for these experiments is shown in Table 5, and examples of synthetic apple tree point clouds generated using L-TreeGen and deformation are illustrated in Fig. 7.

5.2.3. Evaluation metrics

Semantic and instance segmentation performance is evaluated separately following standard procedures from (Dai et al., 2017), (Kolodiazhnyi et al., 2024b), and (Schult et al., 2023). Since semantic segmentation is generally less challenging and serves primarily as a preprocessing step for instance segmentation, a broader set of metrics is reported for semantic segmentation to evaluate its potential integration with instance segmentation heads. These include Intersection over Union (IoU), precision, recall, F1-score, inference speed (FPS), and model parameters.

For instance segmentation, we focus on accuracy, reporting average precision (AP) at IoU thresholds of 25% (AP25) and 50% (AP50), as well as mean AP across thresholds from 50% to 95% with a step size of 5%. Semantic performance of instance networks is also recorded. AP25 and AP50 measure network performance under relatively moderate criteria, while mean AP reflects overall capability under increasingly strict thresholds.

Additionally, for the robustness experiment on 0-shot segmentation with L-TreeGen and deformation, we report both the mean and standard deviation (SD) of mIoU, AP25, AP50, and mean AP across all 12 folds.

5.3. Benchmark results

5.3.1. Semantic segmentation

The semantic segmentation benchmark across 5 datasets for various networks is summarized in Table 6.

- Voxel-based networks generally outperformed pointbased networks: Among all six semantic networks, SPVConv achieved the highest mean mIoU of 86.66% across all datasets. MinkUNet, SCUNet, and PAConv also performed well, with mIoUs of 86.47%, 80.66%, and 81.85%, respectively. In contrast, point-based networks with fewer parameters, such as DGCNN (0.96M) and PointNet++ (1.88M), delivered lower segmentation accuracies. These results indicate that voxel-based methods with sparse convolution, although requiring more parameters, consistently outperform lighter point-based approaches. For example, SPVConv, the lightest and best-performing voxel/hybridbased network, achieved a 5.88% mIoU improvement with 84.89% more parameters compared to PAConv, the best-performing point-based method.
- Efficient sparse convolution backends and skip connections are crucial for SCUNet-like networks: In voxel-based and hybrid methods (e.g., SCUNet, MinkUNet, and SPVConv), the sparse convolution backend plays a key role. In our benchmark, MinkUNet and SPVConv, both using the more efficient Torchsparse backend, achieved better performance with fewer parameters than SCUNet, which uses the SpConv backend.

Additionally, skip connections that propagate information across the voxel-based U-Net, whether via addition or concatenation, proved highly beneficial,

Table 5

Data preparation for L-TreeGen and deformation generation. TG means we only use TG module in L-TreeGen pipeline for generation; TG+VLS03 means we use both TG and VLS modules and set the angular resolution degree to 0.3 to generate more realistic synthetic trees. K_b represent the number of base trees selected from training sets from both orchards, with the ratio in the last column indicating the proportion of the total testing set (26 real trees identical in all benchmarks) represented by K_b .

L-TreeGen	Deformation	Subsets	K_b		Ratio (K_b /Testing set size)
			Orchard1 Orchard2		
TG1	D1	12 (Folds)	3	3	0.23
TG2	D2	2 (L, U bound)	6	6	0.46
TG3	D3	2 (L, U bound)	9	9	0.69
TG4	D4	2 (L, U bound)	12	12	0.92
TG4+VLS03		1 (U bound)	12	12	0.92
TG4+VLS006		1 (U bound)	12	12	0.92
TG4+VLS003		1 (U bound)	12	12	0.92

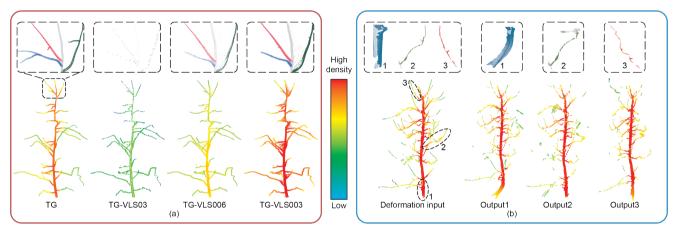


Figure 7: Apple tree point clouds generated from L-TreeGen (a), and deformation (b). For L-TreeGen, the points density and geometry details highly rely on the sensor resolution used in VLS module. For deformation, local-wise transformation are applied to different organs, and the points density are close to the original input point clouds.

and sometimes contributed more to performance than simply increasing hidden layer channels. For instance, MinkUNet concatenates voxel features of varying spatial resolutions before the final linear layer (Fig. 3 (b4)), while SPVConv continuously refines voxel-branch features with point-branch features through addition (Fig. 3 (b6)). Although SCUNet, MinkUNet, and SPVConv share similar voxel-convolution U-Net structures, MinkUNet and SPVConv demonstrated superior ability to capture fine-grained features and accurately segment challenging minor classes (e.g., the mainstem in the SoybeanMVS dataset). In contrast, SCUNet, despite using larger base and convolution channel sizes ([64, 128, 192, 256, 320], Fig. 3 (b5)), failed to detect this class.

 Point convolution significantly improves basic pointbased networks: For point-based methods, PAConv notably improved performance by integrating positionadaptive convolution operations into the PointNet++ backbone, achieving a 17.28 percentage point increase over PointNet++. PAConv also delivered competitive results on the HR3D, Pheno4D, and Pheno4D-RS datasets, with only slight decreases of 0.54, 1.45, and 0.71 percentage points, respectively, compared to the top-performing methods. This demonstrates that point convolution, which captures local geometry more effectively, can substantially enhance lightweight networks.

• Comprehensive evaluation: In terms of inference speed, SCUNet achieved the highest performance at 16.67 frames per second (FPS). On average, voxel-based methods (SCUNet, MinkUNet, and SPVConv) achieved 12.27 FPS, while point-based methods (Point-Net++, DGCNN, and PAConv) averaged 8.22 FPS. Even MinkUNet, the slowest voxel-based method, achieved 9.36 FPS, which is adequate for most downstream applications. A more intuitive comparison of mIoU, inference speed, and network parameters is provided in Fig. 8. These findings suggest voxel-based methods are the optimal choice for integration with

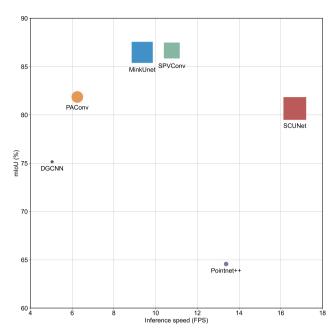


Figure 8: Semantic segmentation benchmarking on six networks across all datasets. Circles: Point-based methods, squares: Voxel-based methods. The radius reflects the model size, larger radius indicates that the model has more parameters (FPS: Frame/Samples per seconds).

instance segmentation, given their advanced feature learning capabilities, faster processing speeds, and acceptable model sizes.

5.3.2. Instance segmentation

Based on the semantic results in Section 5.3.1, we selected the two top-performing semantic networks (MinkUNet and SPVConv) for integration with instance segmentation heads. The benchmark results of instance segmentation across 5 datasets are summarized in Table 7.

• Enhancing semantic heads improves overall performance: Among all instance segmentation networks, SPVFormer achieved the best overall results, with AP25, AP50, and AP scores of 90.04%, 79.11%, and 64.48%, respectively, demonstrating its ability to handle both easy and challenging segmentation requirements. MinkFormer also delivered a competitive performance, ranking second in AP50 and AP with scores of 77.35% and 63.25%. Both models outperformed the current state-of-the-art OneFormer3D by 1.76 and 0.53 percentage points on AP, respectively. These results demonstrate the advantage of combining advanced semantic heads with robust instance heads to further boost performance.

The benefits are even more evident for grouping-based methods. Integrating MinkUNet and SPVConv with the SG instance head led to Mink-SG and SPVConv-SG surpassing the original SG by 17.16 and 12.38

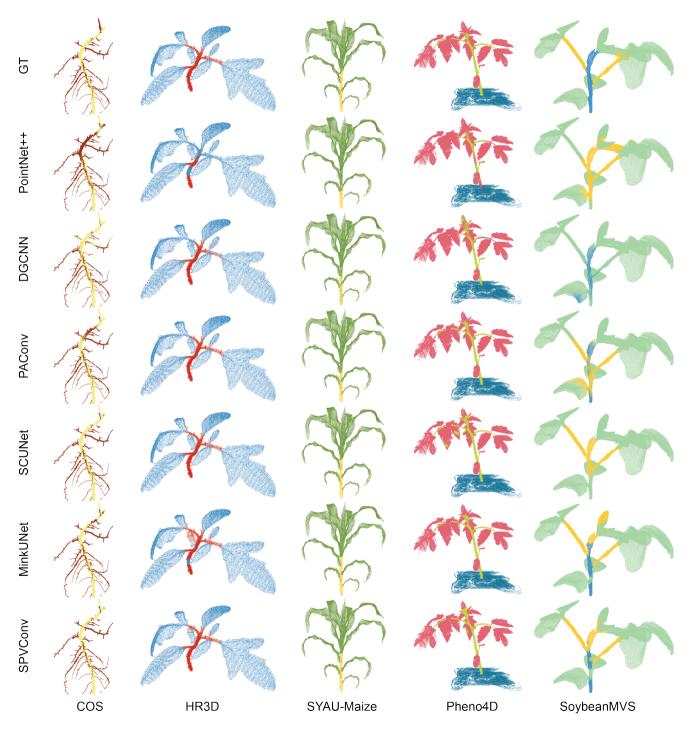


Figure 9: Qualitative results of semantic segmentation.

Table 6Semantic segmentation results. The best results are in boldface.

Network		C	OS	НБ	R3D	SYAU	-Maize]	Pheno4D		Soy	BeanMV	S	Pł	neno4D-R	LS.	SoyB	eanMVS-	RS	Mean
(Params)		trunk	branch	stem	leaf	stem	leaf	ground	stem	leaf	mainstem	stem	leaf	ground	stem	leaf	mainstem	stem	leaf	
PointNet++	Prec	93.27	84.93	74.62	90.69	68.15	97.83	96.13	81.43	90.22	_	48.97	86.57	96.87	80.33	88.11	_	49.09	83.95	
(1.88M)	Rec	92.21	86.83	62.27	94.55	71.08	97.52	99.53	60.96	92.82	_	49.64	88.98	99.54	62.12	92.33	_	42.24	91.05	
	F1	92.74	85.87	67.89	92.58	69.58	97.67	97.80	69.72	91.50	_	49.30	87.76	98.19	70.06	90.17	_	45.41	87.36	
	IoU	86.46	75.24	51.38	86.19	53.36	95.45	95.69	53.52	84.34	_	32.72	78.19	96.44	53.92	82.10	_	29.38	77.56	
	FPS		.46		.53		.78		1.26			1.23			1.81			2.6		13.38
	mIoU	80).85	68	.79	74	.40		77.85			36.97			77.49			35.64		64.57
DGCNN	Prec	91.00	91.44	85.97	95.08	93.10	99.13	99.80	86.70	94.32	54.42	66.20	88.89	99.76	90.73	93.06	65.30	69.51	85.20	
(0.96M)	Rec	96.16	81.19	80.57	96.62	88.35	99.51	99.77	79.93	96.56	30.27	56.51	93.40	99.89	79.91	97.06	17.92	49.04	94.85	
	F1	93.51	86.01	83.19	95.85	90.66	99.32	99.78	83.17	95.42	38.90	60.97	91.09	99.82	84.98	95.02	28.12	57.50	89.76	
	IoU	87.81	75.46	71.21	92.02	82.92	98.65	99.57	71.19	91.25	24.15	43.85	83.64	99.65	73.88	90.51	16.36	40.35	81.43	
	FPS		.91		.61		.33		0.26			0.26			0.4			0.53		5.04
	mIoU	81	.63	81	.62	90	.78		87.34			50.55			88.01			46.05		75.14
PAConv	Prec	95.17	91.85	93.65	98.20	94.81	99.35	99.93	95.74	97.09	73.99	75.14	92.32	99.87	96.27	97.44	81.66	78.43	91.11	
(11.78M)	Rec	95.95	90.37	92.98	98.38	91.32	99.63	99.93	89.92	98.86	24.15	72.34	95.14	99.94	92.70	98.72	17.05	71.33	96.72	
	F1	95.56	91.11	93.31	98.29	93.03	99.49	99.93	92.74	97.97	36.42	73.71	93.71	99.90	94.45	98.08	28.21	74.71	93.83	
	IoU	91.49	83.66	87.46	96.63	86.97	98.98	99.86	86.46	96.02	22.26	58.37	88.16	99.81	89.49	96.22	16.42	59.63	88.38	
	FPS		.03		.48		.95		0.42			0.41			0.64			0.85		6.25
	mIoU	87	7.58	92	.05	92	.98		94.11			56.27			<u>95.18</u>			54.81		81.85
SCUNet	Prec	97.91	89.69	93.81	98.08	96.32	99.59	99.91	92.61	97.79	_	72.68	93.70	99.78	95.15	96.98	_	74.70	91.72	
(43.81M)	Rec	94.42	96.01	92.51	98.43	94.52	99.73	99.97	92.40	97.79	_	80.13	94.23	99.90	91.77	98.12	_	79.00	94.62	
	F1	96.13	92.74	93.15	98.25	95.42	99.66	99.94	92.51	97.79	_	76.22	93.96	99.84	93.43	97.55	_	76.79	93.15	
	IoU	92.55	86.47	87.18	96.57	91.23	99.32	99.88	86.06	95.68	_	61.58	88.62	99.68	87.67	95.21	_	62.32	87.18	
	FPS		3.51		.72		.85		4.87			2.39			4.01			3.37		16.67
	mIoU	89	0.51	91	.88	<u>95</u>	.28		93.87			50.06			94.19			49.83		80.66
MinkUNet	Prec	96.09	94.48	93.57	98.36	97.25	99.46	99.96	95.80	98.08	56.94	81.61	94.97	99.96	97.30	97.58	59.58	83.07	94.81	
(37.87M)	Rec	97.28	92.16	93.62	98.35	92.73	99.80	99.96	93.39	98.82	72.49	76.29	95.71	99.90	93.41	99.12	70.35	77.68	95.66	
	F1	96.68	93.31	93.59	98.35	94.93	99.63	99.96	94.58	98.45	63.78	78.86	95.34	99.93	95.32	98.35	64.52	80.28	95.23	
	IoU	93.57	87.45	87.96	96.76	90.36	99.26	99.91	89.72	96.95	46.82	65.10	91.09	99.86	91.05	96.75	47.62	67.06	90.90	
	FPS		5.06		.62		.74		4.33			2.21			3.51			3.03		9.36
	mIoU	90).51	92	.36	94	.81		<u>95.52</u>			67.67			95.89			<u>68.53</u>		86.47
SPVConv	Prec	96.98	92.15	94.51	98.23	97.23	99.56	99.93	94.94	98.38	61.83	87.11	93.65	99.97	95.71	97.04	63.69	84.97	95.20	
(21.78M)	Rec	95.95	94.09	93.07	98.61	94.06	99.80	99.97	94.34	98.51	63.28	71.92	97.68	99.83	92.19	98.58	71.70	79.59	96.26	
•	F1	96.46	93.11	93.78	98.42	95.62	99.68	99.95	94.64	98.45	62.55	78.79	95.62	99.90	93.92	97.80	67.46	82.19	95.73	
	IoU	93.16	87.10	88.30	96.88	91.60	99.36	99.90	89.82	96.94	45.51	65.00	91.61	99.80	88.54	95.70	50.90	69.77	91.81	
	FPS		7.18		.16		.94		4.31			2.2			3.58			3.11		10.78
	mIoU	<u>90</u>	0.13	92	.59	95	.48		95.56			67.37			94.68			70.83		86.66

percentage points on AP. Mink-SG also slightly outperformed all other models on the COS and HR3D datasets. Additionally, Mink-SG and SPVConv-SG achieved the highest AP on the SoybeanMVS-RS stem (38.14%) and SoybeanMVS-RS leaf (40.88%) classes, outperforming the best transformer-based method's results (achieved by SPVFormer) by 7.55 and 4.22 percentage points, respectively.

- Transformer-based instance networks lead overall performance: On average, transformer-based networks achieved an 11.62 percentage point improvement in AP compared to grouping-based methods. However, the strong feature representations provided by MinkUNet and SPVConv show that groupingbased approaches can still be optimized to perform competitively, especially on challenging datasets like SoybeanMVS-RS.
- Instance networks improve semantic segmentation performance: Table 7 also shows the changes in semantic mIoU when moving from semantic-only training to joint semantic-and-instance training for corresponding networks (e.g., MinkUNet vs. Mink-SG and MinkFormer). For SG and OneFormer3D, which both use a standard structured sparse convolution U-Net backbone, their semantic mIoU was compared with SCUNet. In most cases, mIoU improved with joint training, indicating that optimizing a network for the more complex task of instance segmentation enhances its ability to handle simpler tasks like semantic segmentation.

5.3.3. L-TreeGen and deformation for sim2real learning

We chose SPVFormer to conduct all the experiments in this section given its best overall performance on instance segmentation (Table 7).

• Robustness of L-TreeGen and deformation in 0-shot segmentation: Fig. 11 presents 0-shot segmentation results on mIoU, AP25, AP50, and AP across 12 non-overlapping folds using L-TreeGen and deformation synthetic data for sim2real learning. The deformation-based achieved consistently higher mean values for all metrics. In particular, semantic mIoU and instance AP25 improved significantly by an average of 21.12 and 6.23 percentage points compared to L-TreeGen.

Regarding robustness, deformation-based segmentation exhibited greater stability in semantic mIoU, with a standard deviation (SD) of 0.88. Conversely, L-TreeGen-based segmentation demonstrated more stable instance-level performance, with SD reductions of 1.01, 3.82, and 2.34 on AP25, AP50, and AP, respectively, compared to the deformation.

These differences stem from the generation strategies: L-TreeGen uses the TG module to interpolate geometric features from base trees, producing continuous and complete shapes among all generated data, providing more stable branch instance geometries. In contrast, deformation preserves imperfections from sensor data (e.g., incompleteness or gaps of trunk or branch points) where the instance-level information is less robust (Fig. 7(b)).

O-shot and few-shot performance under varying base tree sizes for synthetic data generation: Fig. 12 shows the lower (LB) and upper-bound (UB) of 0-shot and few-shot performance as the base tree size (K_b = 6, 12, 18, 24) increases. Few-shot results (K_b-shot) are obtained by fine-tuning the network's 0-shot weights with all base trees, providing insight into how base tree diversity affects performance under a fixed synthetic dataset size (150 trees).

In general, 0-shot and few-shot segmentation performance improved with increasing K_b , and UB performance exceeded LB performance, as expected. However, several L-TreeGen-based 0-shot experiments revealed unexpected trends: at certain K_b /test set ratios (0.23, 0.46, 0.69), LB configurations achieved higher semantic performance than their UB counterparts. Besides, AP25, AP50, and AP fluctuated as K_b increased, with performance at a 0.92 ratio matching that at 0.46, despite doubling the number of base trees. These findings indicate:

- Lower-performing base tree configurations may still provide superior results through feature interpolation.
- ii) L-TreeGen is highly sensitive to base tree composition, and simply adding more base trees does not guarantee linear performance improvements, revealing a quality-diversity trade-off.

A key observation emerges when comparing pre and post-fine-tuning performance. For L-TreeGenbased, fine-tuning significantly boosted performance, while deformation-based improvements were modest. Table 8 lists detailed results, showing that although deformation-based 0-shot consistently outperformed L-TreeGen-based, K_b -shot fine-tuning enabled L-TreeGen-based to surpass deformation-based performance by a big margin, especially on instance-level metrics. Remarkably, using only 12 fine-tuning trees $(K_b = 12, \text{ and } 0.46 \text{ of test size})$ achieved comparable results to the vanilla baseline (AP=55.49% achieved by SPVFormer, Table 7), which required 72 real trees. Increasing K_b to 18 and 24 further outperformed this baseline. This demonstrates that using K_b -shot could reduce annotation effort by 83.33% (from 72 to 12 real trees) while maintaining or exceeding baseline performance, underscoring the potential of PM-based sim2real learning for tackling real-world data scarcity challenges.

Table 7Instance segmentation results. The best results are in boldface, and the second best results are underlined. The green and red numbers indicate the mIoU changes from semantic-only networks (Results in Table 6) to instance networks with the corresponding semantic head (e.g., Mink-SG and MinkFormer compared to MinkUNet).

Network			COS	HR3D	SYAU-Maize	Pheno	4D-RS	SoyBear	Mean	
			branch	leaf	leaf	stem	leaf	stem	leaf	
SoftGroup	Ap25		77.25	89.54	92.47	52.06	87.69	59.05	49.52	72.51
	Ap50		47.50	85.82	87.47	39.20	80.60	43.13	27.62	58.76
	Ap		23.52	74.33	68.91	14.99	67.84	25.50	19.03	42.02
	mIoU		91.48	90.13	89.87	89	.69	54	1.46	83.13
	Compared SCUNet	to	(+1.97)	(-1.75)	(-5.41)	(-4	.50)	(+4	4.63)	(-1.01)
Mink-SG	Ap25		87.60	91.71	97.07	96.56	90.48	72.89	70.13	86.63
	Ap50		79.62	89.74	95.45	81.98	82.90	55.89	49.75	76.48
	Ap		56.42	81.72	86.97	44.29	67.57	38.14	39.12	59.18
	mIoU		92.20	92.81	94.37	95	.28	73	3.89	89.71
	Compared	to	(+1.69)	(+0.45)	(-0.44)		61)		5.36)	(+1.29)
	MinkUNet									
SPVConv-SG	Ap25		86.74	91.13	91.91	91.01	88.97	67.42	72.81	84.28
	Ap50		74.85	88.85	83.98	69.87	84.75	50.23	53.30	72.26
	AP		52.02	79.83	74.23	30.44	67.85	35.58	40.88	54.40
	mIoU		91.91	92.74	94.33	95	.76	72	2.80	89.51
	Compared	to	(+1.78)	(+0.15)	(-1.15)	(+1	.08)	(+)	1.97)	(+0.77)
	SPVConv									
OneFormer3D	Ap25		86.21	95.41	98.97	100	89.21	75.32	82.44	89.65
	Ap50		74.96	91.64	97.65	97.33	82.02	43.91	51.01	76.93
	AP		54.53	81.09	92.74	82.27	70.13	24.03	34.27	62.72
	mIoU		92.19	94.12	96.12	96	.43	77	7.51	91.27
	Compared	to	(+2.68)	(+2.24)	(+0.84)	(+2	.24)	(+2	7.68)	(+7.14)
	SCUNet									
MinkFormer	Ap25		86.03	95.12	99.01	100	87.88	75.35	73.83	88.17
	Ap50		74.12	91.78	97.85	100	84.11	43.15	50.47	77.35
	AP		50.62	81.35	94.06	85.68	71.17	25.12	34.74	$\overline{63.25}$
	mIoU		91.71	93.99	95.70	97	.57	76	5.71	91.14
	Compared	to	(+1.2)	(+1.63)	(+0.89)		.68)		8.18)	(+2.72)
	MinkUNet					`		`	,	
SPVFormer	Ap25		88.02	95.39	98.94	100	89.91	79.52	78.48	90.04
	Ap50		76.63	91.36	97.56	100	84.27	51.03	52.94	79.11
	AP		55.49	80.71	92.41	85.12	70.41	30.59	36.66	64.48
	mIoU		91.76	94.05	96.08	97	.75	76	5.46	91.22
	Compared SPVConv	to	(+1.63)	(+1.46)	(+0.6)	(+3	.07)	(+;	5.63)	(+2.48)

Resolution comparison for L-TreeGen-based sim2real learning: Table 9 compares 0-shot and K_b-shot (K_b = 24) performance for TG4 under three different VLS resolutions (VLS03, VLS006, VLS003). In 0-shot experiments, coarse (VLS03) and fine-grained (VLS003) scanning reduced instance-level performance, while VLS006 slightly improved AP50 and AP. After fine-tuning, all configurations achieved comparable results, with VLS006 and VLS003 slightly surpassing the TG4 baseline. These findings indicate that selecting an appropriate resolution is critical for effective sim2real learning, and both overly coarse or overly

fine sensing simulations can hinder generalization. Besides. fine-tuning remains essential for maximizing performance in PM-based sim2real learning.

6. Discussion

6.1. Network design preferences

Based on comprehensive benchmarks conducted across representative plant point cloud datasets, several network design choices have demonstrated superior performance and are recommended for point cloud segmentation in plant

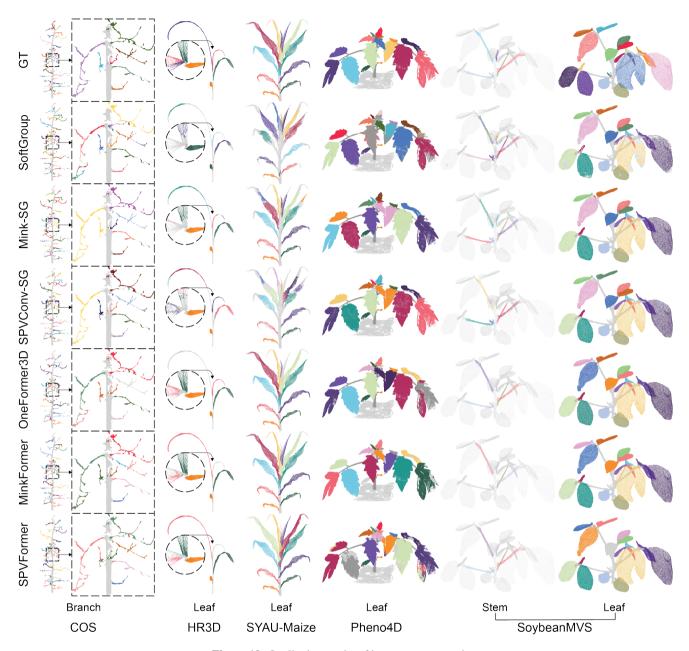


Figure 10: Qualitative results of instance segmentation.

phenotyping. The following subsections summarize these preferences for both semantic and instance segmentation.

6.1.1. Semantic segmentation networks

Our results highlight the superiority of voxel-based methods employing sparse convolutions, particularly SPV-Conv and MinkUNet. These networks excel at capturing multi-scale contextual information from complex yet dense plant point clouds while maintaining computational efficiency through optimized sparse convolution backends (e.g., Torchsparse, Minkowski Engine). Skip connections in these U-Net-like structures further enhance feature representation across multiple scales, which is critical for processing plants with intricate morphology. SPVConv and MinkUNet also

provide a balanced trade-off between segmentation accuracy and computational speed, making them well-suited for diverse downstream tasks. Therefore, SPVConv or MinkUNet are preferred feature extraction backbones when high segmentation accuracy is required.

Although point-based methods exhibit relatively lower performance overall, they remain valuable in scenarios where granule voxelization cannot preserve fine geometric details critical for precise plant morphology characterization. PAConv demonstrated competitive results across several datasets, showing that advanced point convolutions can capture local geometry more effectively and enrich feature representation compared to classic point-MLPs-based backbones. Consequently, point convolution modules

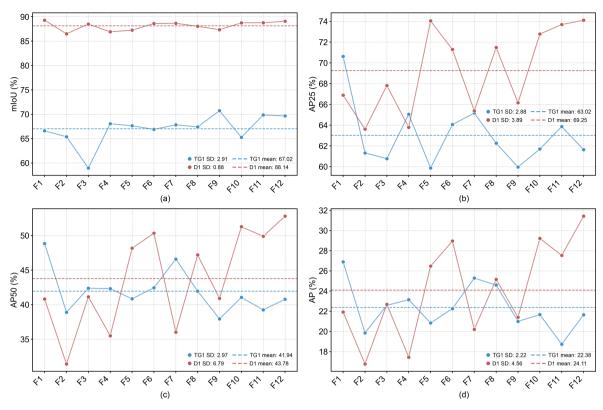


Figure 11: 0-shot performance of using TG (L-TreeGen) and deformation across 12 non-overlap folds on mIoU (a), AP25 (b), AP50 (c), and AP (d). For each fold, we use 6 base trees to generate synthetic data ($K_b = 6$), denoted as TG1 and D1 from L-TreeGen-TG module, and deformation, respectively.

Table 8The upper bound results of 0-shot and few-shot performance using TG and deformation with different number of base trees. We only used TG module from L-TreeGen in this experiment, and it's denoted as TG (TG1,2,3,4 refers to using $K_b = 6, 12, 18, 24$).

K_b	Synthetic Gen.	mIoU		A	P25	A	P50	AP		
		0-shot	K_b -shot							
6	TG1	66.59	90.78	70.62	85.60	48.84	73.02	26.90	50.79	
	D1	89.07	89.44	74.11	77.24	52.80	57.67	31.43	34.66	
12	TG2	68.25	91.48	67.70	86.73	49.55	76.38	26.83	54.29	
	D2	89.82	90.30	79.86	81.65	60.76	65.96	39.02	42.70	
18	TG3	68.42	91.72	70.03	89.76	50.90	77.74	30.48	56.48	
	D3	90.36	91.20	80.39	83.75	64.67	70.06	41.72	48.83	
24	TG4	73.23	91.72	74.33	88.20	54.33	80.07	31.68	60.59	
	D4	89.97	91.68	82.67	86.18	67.95	75.83	45.37	51.01	

are a preferred choice when phenotyping tasks necessitate processing raw point clouds rather than using voxel representations.

However, a key limitation of point-based networks is their incompatibility with many popular instance segmentation heads due to two inherent design characteristics: fixed input size and block-wise downsampling. Point-based networks require raw point clouds to be downsampled into fixed-size inputs to enable parallel processing with structures like MLPs. To retain geometric fidelity, they employ

block-wise sampling, where data is downsampled to a predetermined point size within spatially constrained blocks. While this approach preserves local geometric details, it necessitates a sliding window inference strategy to process individual blocks sequentially and then aggregate the results. This workflow creates a substantial integration barrier with widely adopted voxel-based instance segmentation heads, which operate on dynamically voxelized, full-scale point clouds with direct point-to-voxel mappings.

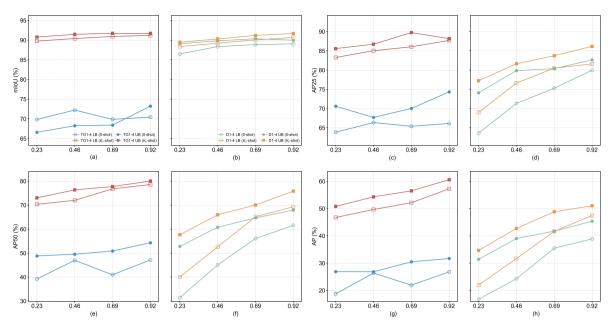


Figure 12: 0-shot and few-shot performance of using TG and deformation across different base tree size ($K_b = 6, 12, 18, 24$), denoted as TG1-4 and D1-4 on mIoU (a), (b), AP25 (c), (d), AP50 (e), (f), and AP (g), (h). Lower bound (LB) performance curves are marked with hollow scatters and upper bound (UB) curves are marked with solid scatters.

Table 9 0-shot and few-shot (with $K_b = 24$) performance under different resolution using L-TreeGen (Using both TG and VLS modules).

Resolution	m	IoU	A	P25	A	P50	AP		
	0-shot	24-shot	0-shot	24-shot	0-shot	24-shot	0-shot	24-shot	
TG4	73.23	91.72	74.33	88.20	54.33	80.07	31.68	60.59	
TG4+VLS03	75.61	91.81	58.97	89.07	30.79	81.12	17.40	59.65	
TG4+VLS006	70.96	91.91	73.01	90.78	54.49	81.45	32.86	61.99	
TG4+VLS003	72.72	91.44	64.19	89.67	45.33	82.02	25.43	61.28	

6.1.2. Instance segmentation networks

Benchmark results indicate that instance segmentation performance is highly dependent on the quality of features extracted by the semantic backbone. Integrating topperforming semantic networks (e.g., SPVConv and MinkUNet) led to substantial improvements for both grouping-based and transformer-based approaches. Networks that combined transformer decoders with strong feature extractors (e.g., SPVFormer, MinkFormer) achieved slightly higher AP across all benchmark datasets, even surpassing leading networks like OneFormer3D. When SPVConv and MinkUNet were integrated into grouping-based methods (e.g., SG variants), the resulting models performed exceptionally well on SoybeanMVS-RS, the most challenging dataset due to its dense stems and leaves. This demonstrates that, for datasets with high object density or severe occlusions, the explicit geometric reasoning of grouping methods can be highly effective in improving segmentation accuracy.

Transformer-based networks generally require less hyperparameter tuning because they involve fewer datasetspecific settings, whereas grouping-based approaches rely heavily on hyperparameters related to point grouping, making careful tuning essential for optimal performance. Among these, the **grouping radius** (Gr^{plant}), the KNN radius threshold for grouping points, and the **class-specific point count threshold** (Gnp_i^{plant} , where $i \in \text{instance classes}$), which determines whether a cluster contains enough points to be classified as a specific instance, are particularly influential. Given that the HR3D dataset includes a wider diversity of plant species and samples, we recommend initializing these parameters for new plant datasets using Gr^{HR3D} and Gnp_i^{HR3D} as references, scaling them proportionally to the mean instance size differences between datasets.

Additionally, semantic mIoU often improved when the semantic task was integrated in an instance network, suggesting that joint training with a powerful decoder enhances the encoder's semantic understanding. A similar phenomenon was reported in (Kolodiazhnyi et al., 2024b), where the integration of both semantic and instance queries improved semantic segmentation performance compared to networks trained with semantic-only queries. These findings

suggest that incorporating an additional instance segmentation task can mitigate overfitting when using transformer-decoder-based architectures for semantic-only tasks. Two strategies for improving semantic performance are therefore recommended: i) replacing simple linear layers with transformer decoders (architecture-level improvement) and ii) jointly training semantic and instance queries (training-level improvement).

In summary, for general-purpose instance segmentation targeting the best overall performance, transformer decoders (e.g., SPVFormer or MinkFormer) built on top of high-performing sparse convolution backbones (SPVConv or MinkUNet) are the most promising choice. For datasets with particularly dense, complex instances, enhancing grouping-based methods (e.g., SG) with these backbones offers a strong alternative, though careful tuning of key hyperparameters is essential. Lastly, Joint semantic and instance training is recommended in both cases to maximize performance.

6.2. PM-based and augmentation-based synthetic training data generation for sim2real learning 6.2.1. 0-shot performance

The deformation approach, which directly transforms existing real-world point clouds, delivered superior 0-shot performance, particularly in semantic segmentation (mIoU). This result suggests that preserving data noise and sensorspecific imperfections is critical for direct sim2real learning without fine-tuning. This finding aligns with domain randomization principles, where introducing non-realistic variability in synthetic data helps bridge the sim2real reality gap effectively (Tobin et al., 2017). While L-TreeGenbased demonstrated greater stability in 0-shot instance-level metric, likely due to its geometrically cleaner procedural model generation, it suffered from a larger initial reality gap, as L-system-based models may not replicate real-world sensor imperfections and textures. Overall, for 0-shot tasks, augmentation-based approaches not only provide stronger performance but are also generally more cost-effective to develop and deploy.

6.2.2. Few-shot performance and annotation efficiency

A key finding is the remarkable effectiveness of L-TreeGen when combined with few-shot fine-tuning. Networks pre-trained on L-TreeGen data (only use TG module) and fine-tuned with a very small subset of real annotated data (as few as 12 trees, reducing annotation requirements by 83.33% compared to vanilla setup) achieved performance comparable to or better than those trained entirely on much larger real datasets. This far exceeded the few-shot gains observed with deformation-based learning. These results indicate that although PM-based sim2real learning introduces a larger initial reality gap, it captures essential structural variability and semantics of the target objects, providing a rich foundation for rapid adaptation with minimal real-world supervision.

6.2.3. Base tree composition and VLS module in L-TreeGen

L-TreeGen results revealed sensitivity to base tree composition, showing that simply increasing the number of base trees does not guarantee proportional performance gains. Striking a balance between base tree quality and diversity is crucial for PM-based modeling and sim2real learning with limited base tree size. Resolution comparisons further emphasized the importance of accurately simulating sensor effects in synthetic data to optimize 0-shot performance, as reducing the initial reality gap, while fine-tuning, remained essential to achieving peak results.

For scenarios lacking robust PM-based synthesis tools or requiring immediate deployment without fine-tuning (pure 0-shot), deformation-based methods or brute-force generation pipelines emphasizing high fidelity and rapid dataset augmentation may be preferred due to their smaller initial reality gap. Conversely, when even a modest amount of annotated real data is available, pre-training on diverse, structurally rich PM-based synthetic data (e.g., L-TreeGen) followed by few-shot fine-tuning offers a highly efficient and effective strategy for achieving state-of-the-art segmentation performance.

7. Conclusion

This study provides a comprehensive review of deep learning (DL)-based 3D plant segmentation, integrating perspectives on datasets, algorithms, and computational workflows to address key barriers limiting its scalability and applicability. By systematically reviewing datasets, benchmarking state-of-the-art segmentation networks, and evaluating the value of synthetic data for sim2real learning, we deliver a clear conclusion of current progress while identifying technical challenges and opportunities for advancement. The introduction of the Plant Segmentation Studio (PSS) establishes a reproducible, extensible platform for community-driven benchmarking, helping to accelerate innovation in this domain.

Our findings highlight the efficacy of sparse convolutional backbones (e.g., SPVConv, MinkUNet) for generalized feature extraction across diverse plant point clouds, while identifying the promise and integration challenges of advanced point-based architectures (e.g., PAConv). Transformer-based instance segmentation demonstrates strong adaptability, whereas grouping-based methods exhibit notable potential for handling complex morphological structures.

Complementary strategies for synthetic data generation further extend these advances: augmentation-based deformation techniques preserve sensing characteristics and are highly effective for 0-shot learning, whereas PM-based L-TreeGen introduces a larger initial reality gap but delivers superior results when used for pre-training and subsequent few-shot fine-tuning. Together, these methods illustrate a practical path toward reducing manual annotation and achieving scalable, high-precision segmentation.

In conclusion, this work bridges a critical gap between cutting-edge algorithmic research and its practical deployment in 3D plant phenotyping. The contributions not only provide immediate tools for domain researchers but also lay the groundwork for future exploration of data-efficient and generalizable DL solutions for 3D plant segmentation. We hope this study will catalyze community efforts to accelerate the success of AI-driven agriculture.

References

- Ao, Z., Wu, F., Hu, S., Sun, Y., Su, Y., Guo, Q., Xin, Q., 2022. Automatic segmentation of stem and leaf components and individual maize plants in field terrestrial lidar data using convolutional neural networks. The Crop Journal Crop phenotyping studies with application to crop monitoring.
- Armeni, I., Sener, O., Zamir, A.R., Jiang, H., Brilakis, I., Fischer, M., Savarese, S., 2016. 3d semantic parsing of large-scale indoor spaces,
- Atkinson, J.A., Pound, M.P., Bennett, M.J., Wells, D.M., 2019. Uncovering the hidden half of plants using new advances in root phenotyping. Current Opinion in Biotechnology Analytical Biotechnology.
- Baa, A., Kontogianni, T., Leibe, B., 2020. Dilated point convolutions: On the receptive field size of point convolutions on 3d point clouds,
- Bao, Y., Tang, L., Srinivasan, S., Schnable, P.S., 2019. Field-based architectural traits characterisation of maize plant using time-of-flight 3d imaging. Biosystems Engineering
- Behley, J., Garbade, M., Milioto, A., Quenzel, J., Behnke, S., Gall, J., Stachniss, C., 2021. Towards 3D LiDAR-based semantic scene understanding of 3D point cloud sequences: The SemanticKITTI Dataset. The International Journal on Robotics Research
- Bernotas, G., Scorza, L.C.T., Hansen, M.F., Hales, I.J., Halliday, K.J., Smith, L.N., Smith, M.L., McCormick, A.J., 2019. A photometric stereo-based 3d imaging system using computer vision and deep learning for tracking plant growth. GigaScience
- Bienert, A., Georgi, L., Kunz, M., von Oheimb, G., Maas, H.G., 2021. Automatic extraction and measurement of individual trees from mobile laser scanning point clouds of forests. Annals of Botany
- Brede, B., Terryn, L., Barbier, N., Bartholomeus, H.M., Bartolo, R., Calders, K., Derroire, G., Krishna Moorthy, S.M., Lau, A., Levick, S.R., Raumonen, P., Verbeeck, H., Wang, D., Whiteside, T., van der Zee, J., Herold, M., 2022. Non-destructive estimation of individual tree biomass: Allometric models, terrestrial and uav laser scanning. Remote Sensing of Environment
- Van den Broeck, W.A.J., Terryn, L., Cherlet, W., Cooper, Z.T., Calders, K., 2023. Three-dimensional deep learning for leaf-wood segmentation of tropical tree point clouds. The International Archives of the Photogrammetry, Remote Sensing and Spatial Information Sciences
- Bryson, M., Wang, F., Allworth, J., 2023. Using synthetic tree data in deep learning-based tree segmentation using lidar point clouds. Remote Sensing
- Çiçek, O., Abdulkadir, A., Lienkamp, S.S., Brox, T., Ronneberger, O., 2016. 3d u-net: Learning dense volumetric segmentation from sparse annotation, in: Medical Image Computing and Computer-Assisted Intervention – MICCAI 2016: 19th International Conference, Athens, Greece, October 17-21, 2016, Proceedings, Part II, Springer-Verlag, Berlin, Heidelberg.
- Chaudhury, A., Boudon, F., Godin, C., 2020. 3d plant phenotyping: All you need is labelled point cloud data, in: Bartoli, A., Fusiello, A. (Eds.), Computer Vision – ECCV 2020 Workshops, Springer International Publishing, Cham.
- Chen, S., Fang, J., Zhang, Q., Liu, W., Wang, X., 2021. Hierarchical aggregation for 3d instance segmentation,
- Chen, X., Kundu, K., Zhu, Y., Berneshawi, A.G., Ma, H., Fidler, S., Urtasun, R., 2015. 3d object proposals for accurate object class detection, in: Cortes, C., Lawrence, N., Lee, D., Sugiyama, M., Garnett, R. (Eds.), Advances in Neural Information Processing Systems,
- Cheng, B., Misra, I., Schwing, A.G., Kirillov, A., Girdhar, R., 2022.

- Choy, C., Gwak, J., Savarese, S., 2019. 4d spatio-temporal convnets: Minkowski convolutional neural networks, in: Proceedings of the IEEE Conference on Computer Vision and Pattern Recognition,
- Chéné, Y., Rousseau, D., Lucidarme, P., Bertheloot, J., Caffier, V., Morel, P., Étienne Belin, Chapeau-Blondeau, F., 2012. On the use of depth camera for 3d phenotyping of entire plants. Computers and Electronics in Agriculture
- Conn, A., Pedmale, U.V., Chory, J., Navlakha, S., 2017a. High-resolution laser scanning reveals plant architectures that reflect universal network design principles. Cell Systems
- Conn, A., Pedmale, U.V., Chory, J., Stevens, C.F., Navlakha, S., 2017b. A statistical description of plant shoot architecture. Current Biology
- Contributors, M., 2020. MMDetection3D: OpenMMLab next-generation platform for general 3D object detection.
- Contributors, S., 2022. Spconv: Spatially sparse convolution library.
- Cournède, P.-H., Letort, V., Mathieu, A., Kang, M. Z., Lemaire, S., Trevezas, S., Houllier, F., de Reffye, P., 2011. Some parameter estimation issues in functional-structural plant modelling. Math. Model. Nat. Phenom.
- Cui, D., Liu, P., Liu, Y., Zhao, Z., Feng, J., 2025. Automated phenotypic analysis of mature soybean using multi-view stereo 3d reconstruction and point cloud segmentation. Agriculture
- Dai, A., Chang, A.X., Savva, M., Halber, M., Funkhouser, T., Nießner, M., 2017. Scannet: Richly-annotated 3d reconstructions of indoor scenes,
- Demol, M., Verbeeck, H., Gielen, B., Armston, J., Burt, A., Disney, M., Duncanson, L., Hackenberg, J., Kükenbrink, D., Lau, A., Ploton, P., Sewdien, A., Stovall, A., Takoudjou, S.M., Volkova, L., Weston, C., Wortel, V., Calders, K., 2022. Estimating forest above-ground biomass with terrestrial laser scanning: Current status and future directions. Methods in Ecology and Evolution
- Du, J., Zhang, Y., Guo, X., Ma, L., Shao, M., Pan, X., Zhao, C., 2016. Micron-scale phenotyping quantification and three-dimensional microstructure reconstruction of vascular bundles within maize stalks based on micro-ct scanning. Functional Plant Biology
- Du, R., Ma, Z., Xie, P., He, Y., Cen, H., 2023. Pst: Plant segmentation transformer for 3d point clouds of rapeseed plants at the podding stage. ISPRS Journal of Photogrammetry and Remote Sensing
- Du, R., Qiu, T., Xu, K., Jiang, Y., 2024. Simulated data enhances threedimensional segmentation-based characterization of real apple trees,
- Dutağacı, H., Rasti, P., Galopin, G., Rousseau, D., 2020. Rose-x: an annotated data set for evaluation of 3d plant organ segmentation methods. Plant Methods
- Easlon, H.M., Bloom, A.J., 2014. Easy leaf area: Automated digital image analysis for rapid and accurate measurement of leaf area. Applications in Plant Sciences
- Engelmann, F., Bokeloh, M., Fathi, A., Leibe, B., Nießner, M., 2020. 3D-MPA: Multi Proposal Aggregation for 3D Semantic Instance Segmentation.
- Engelmann, F., Kontogianni, T., Schult, J., Leibe, B., 2018. Know what your neighbors do: 3d semantic segmentation of point clouds, in: Computer Vision ECCV 2018 Workshops: Munich, Germany, September 8-14, 2018, Proceedings, Part III, Springer-Verlag, Berlin, Heidelberg.
- Esser, F., Klingbeil, L., Zabawa, L., Kuhlmann, H., 2023. Quality analysis of a high-precision kinematic laser scanning system for the use of spatiotemporal plant and organ-level phenotyping in the field. Remote Sensing
- Fang, H., Baret, F., Plummer, S., Schaepman-Strub, G., 2019. An overview of global leaf area index (lai): Methods, products, validation, and applications. Reviews of Geophysics
- Freschet, G.T., Pagès, L., Iversen, C.M., Comas, L.H., Rewald, B., Roumet, C., Klimešová, J., Zadworny, M., Poorter, H., Postma, J.A., et al., 2021. A starting guide to root ecology: strengthening ecological concepts and standardising root classification, sampling, processing and trait measurements. New Phytologist
- Gaillard, M., Miao, C., Schnable, J., Benes, B., 2020. Sorghum segmentation by skeleton extraction, in: Bartoli, A., Fusiello, A. (Eds.), Computer Vision ECCV 2020 Workshops, Springer International Publishing, Cham.

- Gao, L., Liu, Y., Chen, X., Liu, Y., Yan, S., Zhang, M., 2024. Cus3d: A new comprehensive urban-scale semantic-segmentation 3d benchmark dataset. Remote Sensing
- Gao, T., Zhu, F., Paul, P., Sandhu, J., Doku, H.A., Sun, J., Pan, Y., Staswick, P., Walia, H., Yu, H., 2021. Novel 3d imaging systems for high-throughput phenotyping of plants. Remote Sensing
- Ge, X., Wu, S., Wen, W., Shen, F., Xiao, P., Lu, X., Liu, H., Zhang, M., Guo, X., 2025. Lettucep3d: A tool for analysing 3d phenotypes of individual lettuce plants. Biosystems Engineering
- Gené-Mola, J., Sanz-Cortiella, R., Rosell-Polo, J.R., Escolà, A., Gregorio, E., 2021. Pfuji-size dataset: A collection of images and photogrammetry-derived 3d point clouds with ground truth annotations for fuji apple detection and size estimation in field conditions. Data in Brief
- Gong, L., Du, X., Zhu, K., Lin, K., Lou, Q., Yuan, Z., Huang, G., Liu, C., 2021. Panicle-3d: Efficient phenotyping tool for precise semantic segmentation of rice panicle point cloud. Plant Phenomics
- Graham, B., 2015. Sparse 3d convolutional neural networks.
- Graham, B., Engelcke, M., van der Maaten, L., 2018. 3d semantic segmentation with submanifold sparse convolutional networks.
- Guo, Q., Su, Y., Hu, T., Guan, H., Jin, S., Zhang, J., Zhao, X., Xu, K., Wei, D., Kelly, M., Coops, N.C., 2021. Lidar boosts 3d ecological observations and modelings: A review and perspective. IEEE Geoscience and Remote Sensing Magazine
- Guo, Y., Wang, H., Hu, Q., Liu, H., Liu, L., Bennamoun, M., 2020. Deep learning for 3d point clouds: A survey. IEEE Transactions on Pattern Analysis and Machine Intelligence
- Hackel, T., Savinov, N., Ladicky, L., Wegner, J.D., Schindler, K., Pollefeys, M., 2017. Semantic3d.net: A new large-scale point cloud classification benchmark. ISPRS Annals of the Photogrammetry, Remote Sensing and Spatial Information Sciences
- Hahner, M., Dai, D., Liniger, A., Gool, L.V., 2022.
- Hamamoto, T., Uchiyama, H., Shimada, A., Taniguchi, R., 2020. 3d plant growth prediction via image-to-image translation, in: Proceedings of the 15th International Joint Conference on Computer Vision, Imaging and Computer Graphics Theory and Applications (VISIGRAPP 2020) -Volume 5: VISAPP, INSTICC. SciTePress.
- Han, L., Zheng, T., Xu, L., Fang, L., 2020. Occuseg: Occupancy-aware 3d instance segmentation, in: 2020 IEEE/CVF Conference on Computer Vision and Pattern Recognition (CVPR),
- Han, X., Dong, Z., Yang, B., 2021. A point-based deep learning network for semantic segmentation of mls point clouds. ISPRS Journal of Photogrammetry and Remote Sensing
- He, K., Gkioxari, G., Dollár, P., Girshick, R., 2017. Mask r-cnn, in: Proceedings of the IEEE international conference on computer vision,
- He, T., Liu, Y., Shen, C., Wang, X., Sun, C., 2020. Instance-aware embedding for point cloud instance segmentation, in: Computer Vision ECCV 2020: 16th European Conference, Glasgow, UK, August 23–28, 2020, Proceedings, Part XXX, Springer-Verlag, Berlin, Heidelberg.
- He, T., Shen, C., van den Hengel, A., 2021. DyCo3D: Robust Instance Segmentation of 3D Point Clouds through Dynamic Convolution, in: 2021 IEEE/CVF Conference on Computer Vision and Pattern Recognition (CVPR), IEEE Computer Society, Los Alamitos, CA, USA.
- Henrich, J., van Delden, J., Seidel, D., Kneib, T., Ecker, A.S., 2024.
 Treelearn: A deep learning method for segmenting individual trees from ground-based lidar forest point clouds. Ecological Informatics
- Hornik, K., 1991. Approximation capabilities of multilayer feedforward networks. Neural Networks
- Hu, Q., Yang, B., Khalid, S., Xiao, W., Trigoni, N., Markham, A., 2021. Towards semantic segmentation of urban-scale 3d point clouds: A dataset, benchmarks and challenges, in: Proceedings of the IEEE/CVF Conference on Computer Vision and Pattern Recognition (CVPR),
- Hu, Q., Yang, B., Xie, L., Rosa, S., Guo, Y., Wang, Z., Trigoni, N., Markham, A., 2020. Randla-net: Efficient semantic segmentation of large-scale point clouds.
- Huang, J., You, S., 2016.
- Hui, Z., Jin, S., Xia, Y., Wang, L., Yevenyo Ziggah, Y., Cheng, P., 2021.Wood and leaf separation from terrestrial lidar point clouds based on

- mode points evolution. ISPRS Journal of Photogrammetry and Remote Sensing
- Itakura, K., Hosoi, F., 2018. Automatic leaf segmentation for estimating leaf area and leaf inclination angle in 3d plant images. Sensors
- James, S., Wohlhart, P., Kalakrishnan, M., Kalashnikov, D., Irpan, A., Ibarz, J., Levine, S., Hadsell, R., Bousmalis, K., 2018. Sim-to-real via sim-to-sim: Data-efficient robotic grasping via randomized-to-canonical adaptation networks.
- Jiang, L., Zhao, H., Shi, S., Liu, S., Fu, C.W., Jia, J., 2020. Pointgroup: Dual-set point grouping for 3d instance segmentation.
- Jiang, M., Wu, Y., Zhao, T., Zhao, Z., Lu, C., 2018.
- Jiang, Y., Li, C., 2020. Convolutional neural networks for image-based high-throughput plant phenotyping: A review. Plant Phenomics
- Jin, S., Su, Y., Gao, S., Wu, F., Ma, Q., Xu, K., Ma, Q., Hu, T., Liu, J., Pang, S., Guan, H., Zhang, J., Guo, Q., 2020. Separating the structural components of maize for field phenotyping using terrestrial lidar data and deep convolutional neural networks. IEEE Transactions on Geoscience and Remote Sensing
- Jin, S., Su, Y., Wu, F., Pang, S., Gao, S., Hu, T., Liu, J., Guo, Q., 2019.
 Stem-leaf segmentation and phenotypic trait extraction of individual maize using terrestrial lidar data. IEEE Transactions on Geoscience and Remote Sensing
- Jin, S., Sun, X., Wu, F., Su, Y., Li, Y., Song, S., Xu, K., Ma, Q., Baret, F., Jiang, D., Ding, Y., Guo, Q., 2021. Lidar sheds new light on plant phenomics for plant breeding and management: Recent advances and future prospects. ISPRS Journal of Photogrammetry and Remote Sensing
- Khanna, R., Schmid, L., Walter, A., Nieto, J., Siegwart, R., Liebisch, F., 2019. A spatio temporal spectral framework for plant stress phenotyping. Plant Methods
- Kolodiazhnyi, M., Vorontsova, A., Konushin, A., 2024a. Top-down beats bottom-up in 3d instance segmentation,
- Kolodiazhnyi, M., Vorontsova, A., Konushin, A., Rukhovich, D., 2024b. Oneformer3d: One transformer for unified point cloud segmentation, in: Proceedings of the IEEE/CVF Conference on Computer Vision and Pattern Recognition,
- Lambourne, J.G., Willis, K.D., Jayaraman, P.K., Sanghi, A., Meltzer, P., Shayani, H., 2021. Brepnet: A topological message passing system for solid models, in: Proceedings of the IEEE/CVF Conference on Computer Vision and Pattern Recognition (CVPR),
- Landrieu, L., Boussaha, M., 2019.
- Landrieu, L., Simonovsky, M., 2018.
- Lee, J.J., Li, B., Benes, B., 2023. Latent l-systems: Transformer-based tree generator. ACM Trans. Graph.
- Li, D., Ahmed, F., Wang, Z., 2025a. 3d-nod: 3d new organ detection in plant growth by a spatiotemporal point cloud deep segmentation framework.
- Li, D., Li, J., Xiang, S., Pan, A., 2022a. Psegnet: Simultaneous semantic and instance segmentation for point clouds of plants. Plant Phenomics
- Li, D., Liu, L., Xu, S., Jin, S., 2024a. Trackplant3d: 3d organ growth tracking framework for organ-level dynamic phenotyping. Computers and Electronics in Agriculture
- Li, D., Shi, G., Li, J., Chen, Y., Zhang, S., Xiang, S., Jin, S., 2022b. Plantnet: A dual-function point cloud segmentation network for multiple plant species. ISPRS Journal of Photogrammetry and Remote Sensing
- Li, D., Wei, Y., Zhu, R., 2023. A comparative study on point cloud downsampling strategies for deep learning-based crop organ segmentation. Plant Methods
- Li, D., Zhou, Z., Wei, Y., 2024b. Unsupervised shape-aware som downsampling for plant point clouds. ISPRS Journal of Photogrammetry and Remote Sensing
- Li, X., Park, J., Reberg-Horton, C., Mirsky, S., Lobaton, E., Xiang, L., 2024c. Photorealistic arm robot simulation for 3d plant reconstruction and automatic annotation using unreal engine 5, in: 2024 IEEE/CVF Conference on Computer Vision and Pattern Recognition Workshops (CVPRW).
- Li, Y., Wen, W., Miao, T., Wu, S., Yu, Z., Wang, X., Guo, X., Zhao, C., 2022c. Automatic organ-level point cloud segmentation of maize shoots

- by integrating high-throughput data acquisition and deep learning. Computers and Electronics in Agriculture
- Li, Z., Su, Y., 2025. A 3D point cloud instance segmentation method for strawberry based on SGC, in: Xu, X., bin Mohd Zain, A. (Eds.), International Conference on Computer Graphics, Artificial Intelligence, and Data Processing (ICCAID 2024), International Society for Optics and Photonics. SPIE.
- Li, Z., Wang, S., Su, Y., Yu, D., 2025b. A method for measuring strawberry leaf area based on three-dimensional point cloud instance segmentation. IEEE Access
- Liang, X., Kankare, V., Hyyppä, J., Wang, Y., Kukko, A., Haggrén, H., Yu, X., Kaartinen, H., Jaakkola, A., Guan, F., Holopainen, M., Vastaranta, M., 2016. Terrestrial laser scanning in forest inventories. ISPRS Journal of Photogrammetry and Remote Sensing Theme issue 'State-of-the-art in photogrammetry, remote sensing and spatial information science'.
- Liang, Z., Li, Z., Xu, S., Tan, M., Jia, K., 2021. Instance segmentation in 3d scenes using semantic superpoint tree networks, in: Proceedings of the IEEE/CVF International Conference on Computer Vision,
- Liao, Y., Xie, J., Geiger, A., 2021. KITTI-360: A novel dataset and benchmarks for urban scene understanding in 2d and 3d.
- Lindenmayer, A., 1968. Mathematical models for cellular interactions in development i. filaments with one-sided inputs. Journal of Theoretical Biology
- Liu, Z., Tang, H., Lin, Y., Han, S., 2019. Point-voxel cnn for efficient 3d deep learning.
- Long, J., Shelhamer, E., Darrell, T., 2015. Fully convolutional networks for semantic segmentation, in: 2015 IEEE Conference on Computer Vision and Pattern Recognition (CVPR), IEEE Computer Society, Los Alamitos, CA, USA.
- Lowry, G.V., Giraldo, J.P., Steinmetz, N.F., Avellan, A., Demirer, G.S., Ristroph, K.D., Wang, G.J., Hendren, C.O., Alabi, C.A., Caparco, A., et al., 2024. Towards realizing nano-enabled precision delivery in plants. Nature Nanotechnology
- Luo, L., Jiang, X., Yang, Y., Samy, E.R.A., Lefsrud, M., Hoyos-Villegas, V., Sun, S., 2023. Eff-3dpseg: 3d organ-level plant shoot segmentation using annotation-efficient deep learning. Plant Phenomics
- Ma, X., Zhu, K., Guan, H., Feng, J., Yu, S., Liu, G., 2019. High-throughput phenotyping analysis of potted soybean plants using colorized depth images based on a proximal platform. Remote Sensing
- Ma, Z., Du, R., Xie, J., Sun, D., Fang, H., Jiang, L., Cen, H., 2023. Phenotyping of silique morphology in oilseed rape using skeletonization with hierarchical segmentation. Plant Phenomics
- Marks, E., Bömer, J., Magistri, F., Sag, A., Behley, J., Stachniss, C., 2024.Bonnbeetclouds3d: A dataset towards point cloud-based organ-level phenotyping of sugar beet plants under real field conditions, in: 2024 IEEE/RSJ International Conference on Intelligent Robots and Systems (IROS)
- Maturana, D., Scherer, S., 2015. Voxnet: A 3d convolutional neural network for real-time object recognition, in: 2015 IEEE/RSJ International Conference on Intelligent Robots and Systems (IROS),
- Měch, R., Prusinkiewicz, P., 1996. Visual models of plants interacting with their environment, in: Proceedings of the 23rd annual conference on Computer graphics and interactive techniques,
- Mertoğlu, K., Şalk, Y., Sarıkaya, S.K., Turgut, K., Evrenosoğlu, Y., Çevikalp, H., Gerek, Ö.N., Dutağacı, H., Rousseau, D., 2023. Planest-3d: A new annotated data set of 3d color point clouds of plants, in: 2023 31st Signal Processing and Communications Applications Conference (SIU),
- Mirande, K., Godin, C., Tisserand, M., Charlaix, J., Besnard, F., Hétroy-Wheeler, F., 2022. A graph-based approach for simultaneous semantic and instance segmentation of plant 3d point clouds. Frontiers in Plant Science
- Mkaouar, A., Kallel, A., Rabah, Z.B., Chahed, T.S., 2021. Joint estimation of leaf area density and leaf angle distribution using tls point cloud for forest stands. IEEE Journal of Selected Topics in Applied Earth Observations and Remote Sensing
- Mo, K., Zhu, S., Chang, A.X., Yi, L., Tripathi, S., Guibas, L.J., Su, H., 2019.PartNet: A large-scale benchmark for fine-grained and hierarchical part-level 3D object understanding,

- Niemeyer, J., Rottensteiner, F., Soergel, U., 2012. Conditional random fields for lidar point cloud classification in complex urban areas. ISPRS Annals of Photogrammetry, Remote Sensing and Spatial Information Sciences
- Patel, A.K., Park, E.S., Lee, H., Priya, G.G.L., Kim, H., Joshi, R., Arief, M.A.A., Kim, M.S., Baek, I., Cho, B.K., 2023. Deep learning-based plant organ segmentation and phenotyping of sorghum plants using lidar point cloud. IEEE Journal of Selected Topics in Applied Earth Observations and Remote Sensing
- Prusinkiewicz, P., 1986. Graphical applications of l-systems, in: Proceedings on Graphics Interface '86/Vision Interface '86, Canadian Information Processing Society, CAN.
- Prusinkiewicz, P., Hammel, M.S., Mjolsness, E., 1993. Animation of plant development, in: Proceedings of the 20th Annual Conference on Computer Graphics and Interactive Techniques, Association for Computing Machinery, New York, NY, USA.
- Prusinkiewicz, P., Lindenmayer, A., 1990. The algorithmic beauty of plants. Qi, C.R., Su, H., Mo, K., Guibas, L.J., 2017a. Pointnet: Deep learning on point sets for 3d classification and segmentation, in: Proceedings of the IEEE conference on computer vision and pattern recognition,
- Qi, C.R., Yi, L., Su, H., Guibas, L.J., 2017b. Pointnet++: Deep hierarchical feature learning on point sets in a metric space.
- Qian, B., Huang, W., Xie, D., Ye, H., Guo, A., Pan, Y., Jin, Y., Xie, Q., Jiao, Q., Zhang, B., Ruan, C., Xu, T., Zhang, Y., Nie, T., 2023. Coupled maize model: A 4d maize growth model based on growing degree days. Computers and Electronics in Agriculture
- Qiu, Q., Sun, N., Bai, H., Wang, N., Fan, Z., Wang, Y., Meng, Z., Li, B., Cong, Y., 2019. Field-based high-throughput phenotyping for maize plant using 3d lidar point cloud generated with a "phenomobile". Frontiers in Plant Science
- Qiu, R., Miao, Y., Zhang, M., Li, H., 2021. Detection of the 3d temperature characteristics of maize under water stress using thermal and rgb-d cameras. Computers and Electronics in Agriculture
- Qiu, T., Du, R., Spine, N., Cheng, L., Jiang, Y., 2025.
- Qiu, T., Wang, T., Han, T., Kuehn, K., Cheng, L., Meng, C., Xu, X., Xu, K., Yu, J., 2024a. Appleqsm: Geometry-based 3d characterization of apple tree architecture in orchards. Plant Phenomics
- Qiu, T., Zoubi, A., Spine, N., Cheng, L., Jiang, Y., 2024b. (real2sim)-1: 3d branch point cloud completion for robotic pruning in apple orchards, in: 2024 IEEE/RSJ International Conference on Intelligent Robots and Systems (IROS),
- Rabbani, T., Heuvel, F., Vosselman, G., 2006. Segmentation of point clouds using smoothness constraint. International Archives of Photogrammetry, Remote Sensing and Spatial Information Sciences
- Ren, Z., Sudderth, E.B., 2016. Three-dimensional object detection and layout prediction using clouds of oriented gradients, in: 2016 IEEE Conference on Computer Vision and Pattern Recognition (CVPR),
- Rusu, R., Marton, Z., Blodow, N., Beetz, M., 2008. Learning informative point classes for the acquisition of object model maps,
- Saeed, F., Sun, S., Rodriguez-Sanchez, J., Snider, J., Liu, T., Li, C., 2023. Cotton plant part 3d segmentation and architectural trait extraction using point voxel convolutional neural networks. Plant methods
- Schult, J., Engelmann, F., Hermans, A., Litany, O., Tang, S., Leibe, B., 2023.
- Schunck, D., Magistri, F., Rosu, R.A., Cornelißen, A., Chebrolu, N., Paulus, S., Léon, J., Behnke, S., Stachniss, C., Kuhlmann, H., Klingbeil, L., 2021. Pheno4d: A spatio-temporal dataset of maize and tomato plant point clouds for phenotyping and advanced plant analysis. PLOS ONE
- Shen, X., Huang, Q., Wang, X., Li, J., Xi, B., 2022. A deep learning-based method for extracting standing wood feature parameters from terrestrial laser scanning point clouds of artificially planted forest. Remote Sensing
- Shen, Y., Feng, C., Yang, Y., Tian, D., 2018. Mining point cloud local structures by kernel correlation and graph pooling,
- Simpson, M.G., 2019. 9 plant morphology, in: Simpson, M.G. (Ed.), Plant Systematics (Third Edition). third edition ed.. Academic Press,
- Smith, A.R., 1984. Plants, fractals, and formal languages. SIGGRAPH Comput. Graph.
- Song, H., Wen, W., Wu, S., Guo, X., 2025. Comprehensive review on 3d point cloud segmentation in plants. Artificial Intelligence in Agriculture

- Song, P., Li, Z., Yang, M., Shao, Y., Pu, Z., Yang, W., Zhai, R., 2023. Dynamic detection of three-dimensional crop phenotypes based on a consumer-grade rgb-d camera. Frontiers in Plant Science
- Song, Q., Srinivasan, V., Long, S., Zhu, X., 2019. Decomposition analysis on soybean productivity increase under elevated co2 using 3d canopy model reveals synergestic effects of co2 and light in photosynthesis. Annals of botany
- Staedler, Y.M., Masson, D., Schönenberger, J., 2013. Plant tissues in 3d via x-ray tomography: Simple contrasting methods allow high resolution imaging. PLOS ONE
- Stausberg, L., Jost, B., Klingbeil, L., Kuhlmann, H., 2024. A 3d surface reconstruction pipeline for plant phenotyping. Remote Sensing
- Stava, O., Pirk, S., Kratt, J., Chen, B., Měch, R., Deussen, O., Benes, B., 2014. Inverse procedural modelling of trees, in: Computer Graphics Forum, Wiley Online Library.
- Sun, J., Qing, C., Tan, J., Xu, X., 2022.
- Sun, P., Kretzschmar, H., Dotiwalla, X., Chouard, A., Patnaik, V., Tsui, P., Guo, J., Zhou, Y., Chai, Y., Caine, B., et al., 2020a. Scalability in perception for autonomous driving: Waymo open dataset, in: Proceedings of the IEEE/CVF conference on computer vision and pattern recognition,
- Sun, S., Li, C., Chee, P.W., Paterson, A.H., Jiang, Y., Xu, R., Robertson, J.S., Adhikari, J., Shehzad, T., 2020b. Three-dimensional photogrammetric mapping of cotton bolls in situ based on point cloud segmentation and clustering. ISPRS Journal of Photogrammetry and Remote Sensing
- Sun, S., Li, C., Paterson, A.H., 2017. In-field high-throughput phenotyping of cotton plant height using lidar. Remote Sensing
- Sun, S., Li, C., Paterson, A.H., Jiang, Y., Xu, R., Robertson, J.S., Snider, J.L., Chee, P.W., 2018. In-field high throughput phenotyping and cotton plant growth analysis using lidar. Frontiers in Plant Science
- Sun, W., Rebain, D., Liao, R., Tankovich, V., Yazdani, S., Yi, K., Tagliasacchi, A., 2023a. Neuralbf: Neural bilateral filtering for top-down instance segmentation on point clouds.
- Sun, Y., Zhang, Z., Sun, K., Li, S., Yu, J., Miao, L., Zhang, Z., Li, Y., Zhao, H., Hu, Z., Xin, D., Chen, Q., Zhu, R., 2023b. Soybean-mvs: Annotated three-dimensional model dataset of whole growth period soybeans for 3d plant organ segmentation. Agriculture
- Tang, H., Liu, Z., Li, X., Lin, Y., Han, S., 2022. TorchSparse: Efficient Point Cloud Inference Engine,
- Tang, H., Liu, Z., Zhao, S., Lin, Y., Lin, J., Wang, H., Han, S., 2020.Searching efficient 3d architectures with sparse point-voxel convolution,
- Tang, H., Yang, S., Liu, Z., Hong, K., Yu, Z., Li, X., Dai, G., Wang, Y., Han, S., 2023a. TorchSparse++: Efficient Point Cloud Engine,
- Tang, H., Yang, S., Liu, Z., Hong, K., Yu, Z., Li, X., Dai, G., Wang, Y., Han, S., 2023b. Torchsparse++: Efficient training and inference framework for sparse convolution on gpus,
- Tang, S., Ao, Z., Li, Y., Huang, H., Xie, L., Wang, R., Wang, W., Guo, R., 2024. Treenet3d: A large scale tree benchmark for 3d tree modeling, carbon storage estimation and tree segmentation. International Journal of Applied Earth Observation and Geoinformation
- Tchapmi, L., Choy, C., Armeni, I., Gwak, J., Savarese, S., 2017. Segcloud: Semantic segmentation of 3d point clouds,
- Terryn, L., Calders, K., Disney, M., Origo, N., Malhi, Y., Newnham, G., Raumonen, P., Å kerblom, M., Verbeeck, H., 2020. Tree species classification using structural features derived from terrestrial laser scanning. ISPRS Journal of Photogrammetry and Remote Sensing
- Thomas, H., Qi, C.R., Deschaud, J.E., Marcotegui, B., Goulette, F., Guibas, L.J., 2019. Kpconv: Flexible and deformable convolution for point clouds.
- Tiozzo Fasiolo, D., Scalera, L., Maset, E., Gasparetto, A., 2023. Towards autonomous mapping in agriculture: A review of supportive technologies for ground robotics. Robotics and Autonomous Systems
- Tobin, J., Fong, R., Ray, A., Schneider, J., Zaremba, W., Abbeel, P., 2017. Domain randomization for transferring deep neural networks from simulation to the real world, in: 2017 IEEE/RSJ International Conference on Intelligent Robots and Systems (IROS), IEEE Press.
- Tong, H., Gong, D., Tian, Z., Shen, C., 2020. Learning and Memorizing Representative Prototypes for 3D Point Cloud Semantic and Instance Segmentation.

- Tracy, S.R., Nagel, K.A., Postma, J.A., Fassbender, H., Wasson, A., Watt, M., 2020. Crop improvement from phenotyping roots: highlights reveal expanding opportunities. Trends in plant science
- Turgut, K., Dutagaci, H., Galopin, G., Rousseau, D., 2022. Segmentation of structural parts of rosebush plants with 3d point-based deep learning methods. Plant Methods
- Varney, N., Asari, V.K., Graehling, Q., 2020. Dales: A large-scale aerial lidar data set for semantic segmentation, in: 2020 IEEE/CVF Conference on Computer Vision and Pattern Recognition Workshops (CVPRW),
- Vos, J., Evers, J.B., Buck-Sorlin, G.H., Andrieu, B., Chelle, M., De Visser, P.H., 2010. Functional–structural plant modelling: a new versatile tool in crop science. Journal of experimental Botany
- Vu, T., Kim, K., Luu, T.M., Nguyen, X.T., Yoo, C.D., 2022. Softgroup for 3d instance segmentation on 3d point clouds,
- Vu, T., Kim, K., Nguyen, T., Luu, T.M., Kim, J., Yoo, C.D., 2024. Scalable softgroup for 3d instance segmentation on point clouds. IEEE Trans. Pattern Anal. Mach. Intell.
- Wang, D., 2020. Unsupervised semantic and instance segmentation of forest point clouds. ISPRS Journal of Photogrammetry and Remote Sensing
- Wang, G., Laga, H., Jia, J., Xie, N., Tabia, H., 2018a. Statistical modeling of the 3d geometry and topology of botanical trees. Computer Graphics Forum
- Wang, L., Huang, Y., Hou, Y., Zhang, S., Shan, J., 2019a. Graph attention convolution for point cloud semantic segmentation, in: 2019 IEEE/CVF Conference on Computer Vision and Pattern Recognition (CVPR).
- Wang, L., Miao, Y., Han, Y., Li, H., Zhang, M., Peng, C., 2023. Extraction of 3d distribution of potato plant cwsi based on thermal infrared image and binocular stereovision system. Frontiers in Plant Science
- Wang, L., Zheng, L., Wang, M., 2022a. 3d point cloud instance segmentation of lettuce based on partnet, in: Proceedings of the IEEE/CVF Conference on Computer Vision and Pattern Recognition (CVPR) Workshops.
- Wang, M., Deng, W., 2018. Deep visual domain adaptation: A survey. Neurocomputing
- Wang, S., Suo, S., Ma, W.C., Pokrovsky, A., Urtasun, R., 2018b. Deep parametric continuous convolutional neural networks, in: 2018 IEEE/CVF Conference on Computer Vision and Pattern Recognition,
- Wang, W., Yu, R., Huang, Q., Neumann, U., 2018c. Sgpn: Similarity group proposal network for 3d point cloud instance segmentation,
- Wang, X., Kong, T., Shen, C., Jiang, Y., Li, L., 2020a. Solo: Segmenting objects by locations, in: Computer Vision ECCV 2020: 16th European Conference, Glasgow, UK, August 23–28, 2020, Proceedings, Part XVIII, Springer-Verlag, Berlin, Heidelberg.
- Wang, X., Zhang, R., Kong, T., Li, L., Shen, C., 2020b. Solov2: Dynamic and fast instance segmentation, in: Larochelle, H., Ranzato, M., Hadsell, R., Balcan, M., Lin, H. (Eds.), Advances in Neural Information Processing Systems, Curran Associates, Inc..
- Wang, Y., Fang, H., 2020. Estimation of lai with the lidar technology: A review. Remote Sensing
- Wang, Y., Hu, S., Ren, H., Yang, W., Zhai, R., 2022b. 3dphenomys: A low-cost 3d tomato phenotyping pipeline using 3d reconstruction point cloud based on multiview images. Agronomy
- Wang, Y., Sun, Y., Liu, Z., Sarma, S.E., Bronstein, M.M., Solomon, J.M., 2019b. Dynamic graph cnn for learning on point clouds.
- Wang, Z., Verboven, P., Nicolai, B., 2017. Contrast-enhanced 3d micro-ct of plant tissues using different impregnation techniques. Plant methods
- Wang, Z., Wang, K., Yang, F., Pan, S., Han, Y., 2018d. Image segmentation of overlapping leaves based on chan-vese model and sobel operator. Information Processing in Agriculture
- Wang, Z., Zhang, L., Fang, T., Mathiopoulos, P.T., Tong, X., Qu, H., Xiao, Z., Li, F., Chen, D., 2015. A multiscale and hierarchical feature extraction method for terrestrial laser scanning point cloud classification. IEEE Transactions on Geoscience and Remote Sensing
- Weinmann, M., Schmidt, A., Mallet, C., Hinz, S., Rottensteiner, F., Jutzi,
 B., 2015. Contextual classification of point cloud data by exploiting individual 3d neighborhoods. ISPRS Annals of the Photogrammetry,
 Remote Sensing and Spatial Information Sciences

- Winiwarter, L., Esmorís Pena, A.M., Weiser, H., Anders, K., Martínez Sánchez, J., Searle, M., Höfle, B., 2022. Virtual laser scanning with helios++: A novel take on ray tracing-based simulation of topographic full-waveform 3d laser scanning. Remote Sensing of Environment
- Wu, S., Wen, W., Gou, W., Lu, X., Zhang, W., Zheng, C., Xiang, Z., Chen, L., Guo, X., 2022. A miniaturized phenotyping platform for individual plants using multi-view stereo 3d reconstruction. Frontiers in Plant Science
- Wu, S., Wen, W., Wang, Y., Fan, J., Wang, C., Gou, W., Guo, X., 2020.
 Mvs-pheno: A portable and low-cost phenotyping platform for maize shoots using multiview stereo 3d reconstruction. Plant Phenomics
- Wu, W., Qi, Z., Li, F., 2019. Pointconv: Deep convolutional networks on 3d point clouds,
- Wyatt, J., 2016. Grain and plant morphology of cereals and how characters can be used to identify varieties, in: Wrigley, C., Corke, H., Seetharaman, K., Faubion, J. (Eds.), Encyclopedia of Food Grains (Second Edition). second edition ed.. Academic Press, Oxford,
- Xi, Z., Hopkinson, C., Rood, S.B., Peddle, D.R., 2020. See the forest and the trees: Effective machine and deep learning algorithms for wood filtering and tree species classification from terrestrial laser scanning. ISPRS Journal of Photogrammetry and Remote Sensing
- Xiang, B., Wielgosz, M., Kontogianni, T., Peters, T., Puliti, S., Astrup, R., Schindler, K., 2024. Automated forest inventory: Analysis of highdensity airborne lidar point clouds with 3d deep learning. Remote Sensing of Environment
- Xiao, S., Chai, H., Shao, K., Shen, M., Wang, Q., Wang, R., Sui, Y., Ma, Y., 2020. Image-based dynamic quantification of aboveground structure of sugar beet in field. Remote Sensing
- Xie, P., Du, R., Ma, Z., Cen, H., 2023. Generating 3d multispectral point clouds of plants with fusion of snapshot spectral and rgb-d images. Plant Phenomics
- Xie, P., Ma, Z., Du, R., Yang, X., Jiang, Y., Cen, H., 2024. An unmanned ground vehicle phenotyping-based method to generate three-dimensional multispectral point clouds for deciphering spatial heterogeneity in plant traits. Molecular Plant
- Xie, Y., Tian, J., Zhu, X.X., 2020. Linking points with labels in 3d: A review of point cloud semantic segmentation. IEEE Geoscience and Remote Sensing Magazine
- Xin, B., Sun, J., Bartholomeus, H., Kootstra, G., 2023. 3d dataaugmentation methods for semantic segmentation of tomato plant parts. Frontiers in Plant Science
- Xu, M., Ding, R., Zhao, H., Qi, X., 2021. Paconv: Position adaptive convolution with dynamic kernel assembling on point clouds,
- Xu, R., Li, C., 2022. A review of high-throughput field phenotyping systems: Focusing on ground robots. Plant Phenomics
- Yang, B., Wang, J., Clark, R., Hu, Q., Wang, S., Markham, A., Trigoni, N., 2019. Learning object bounding boxes for 3D instance segmentation on point clouds.
- Yang, W., Feng, H., Zhang, X., Zhang, J., Doonan, J.H., Batchelor, W.D., Xiong, L., Yan, J., 2020. Crop phenomics and high-throughput phenotyping: Past decades, current challenges, and future perspectives. Molecular Plant
- Yang, X., Miao, T., Tian, X., Wang, D., Zhao, J., Lin, L., Zhu, C., Yang, T., Xu, T., 2024. Maize stem-leaf segmentation framework based on deformable point clouds. ISPRS Journal of Photogrammetry and Remote Sensing
- Yi, L., Kim, V.G., Ceylan, D., Shen, I.C., Yan, M., Su, H., Lu, C., Huang, Q., Sheffer, A., Guibas, L., 2016. A scalable active framework for region annotation in 3d shape collections. ACM Trans. Graph.
- Yi, L., Zhao, W., Wang, H., Sung, M., Guibas, L.J., 2019. Gspn: Generative shape proposal network for 3d instance segmentation in point cloud, in: 2019 IEEE/CVF Conference on Computer Vision and Pattern Recognition (CVPR).
- You, A., Grimm, C., Davidson, J., 2022. Optical flow-based branch segmentation for complex orchard environments,
- Yun, T., Eichhorn, M.P., Jin, S., Yuan, X., Fang, W., Lu, X., Wang, X., Zhang, H., 2025. A framework for phenotyping rubber trees under intense wind stress using laser scanning and digital twin technology.

- Agricultural and Forest Meteorology
- Zarei, A., Li, B., Schnable, J.C., Lyons, E., Pauli, D., Barnard, K., Benes,B., 2024. Plantsegnet: 3d point cloud instance segmentation of nearbyplant organs with identical semantics. Computers and Electronics in Agriculture
- Zhai, A.J., Wang, X., Li, K., Jiang, Z., Zhou, J., Wang, S., Jin, Z., Guan, K., Wang, S., 2024.
- Zhang, S., Song, Y., Ou, R., Liu, Y., Li, S., Lu, X., Xu, S., Su, Y., Jiang,
 D., Ding, Y., Xia, H., Guo, Q., Wu, J., Zhang, J., Wang, J., Jin, S., 2024.
 Scag: A stratified, clustered, and growing-based algorithm for soybean branch angle extraction and ideal plant architecture evaluation. Plant Phenomics
- Zhao, H., Jiang, L., Fu, C.W., Jia, J., 2019. Pointweb: Enhancing local neighborhood features for point cloud processing, in: 2019 IEEE/CVF Conference on Computer Vision and Pattern Recognition (CVPR),
- Zheng, G., Moskal, L.M., Kim, S.H., 2013. Retrieval of effective leaf area index in heterogeneous forests with terrestrial laser scanning. IEEE Transactions on Geoscience and Remote Sensing
- Zhu, B., Liu, F., Xie, Z., Guo, Y., Li, B., Ma, Y., 2020. Quantification of light interception within image-based 3-d reconstruction of sole and intercropped canopies over the entire growth season. Annals of botany
- Zhu, J., Zhai, R., Ren, H., Xie, K., Du, A., He, X., Cui, C., Wang, Y., Ye, J., Wang, J., et al., 2024. Crops3d: a diverse 3d crop dataset for realistic perception and segmentation toward agricultural applications. Scientific Data
- Zolanvari, I., Ruano, S., Rana, A., Cummins, A., Smolic, A., Da Silva, R., Rahbar, M., 2019.